rijksuniversiteit
groningen

University of Groningen

Faculty of Science & Engineering

BSc Industrial Engineering & Management

Inverted Pendulum Demonstrator

Final Report

First Supervisor: Martin Stokroos

Second Supervisor: Mauricio Munoz Arias

19th June 2019

Vlada Sonic

S3164160

Acknowledgements

I would like to convey my special thanks to Martin Stokroos and Pablo Borja Rosales for the knowledge and help with the understanding of the software and hardware and further guidance with the project as well as my family and friends who supported me and believed in me throughout my BSc degree.

Sincerely,

Vlada Sonic
June 2019

În memoria lui tăticu

Abstract

Throughout the years, the Inverted Pendulum allowed Control Systems Engineers to test most of the Classical as well as Innovative Control Theories in its settings due to its real-life applications and fast, insightful response.

University of Groningen wants to test the behaviour of the Inverted Pendulum by use of Bachelor taught models of control in a new system setting. As the system is a highly unstable and non-linear one, it is considered as complex.

The core of the thesis lies in embedding the electrical and mechanical components to work together. Based on the processing of the readouts from the sensors, the control law runs on the dSPACE Hardware and reacts to changes by driving the DC-motor forward or backward. External factors such as friction are expected to affect the performance of the system. In this thesis the LQR current as well as voltage control of the DC-motor are implemented to bring the system to the desired upward location of the pendulum. The control law was obtained in MATLAB and implemented in Simulink.

The paper includes hardware and system description, state-space representations, transfer-function derivation, analysis of the dynamics of the system, simulations, validation, performance comparison of the chosen methods and limitations. Due to the non-linearity of the setup, the simulated results differ from the real-life experiments. The testing phase resulted in success and in an upward stability of the pendulum.

Table of Contents

Nomenclature

Abbreviations	
Long	*Short*
Inverted Pendulum	IP
Equation	Eq.
Direct Current	DC
Analog to Digital; Digital to Analog Converter	A/DC; D/AC
Operational Amplifier	Op-amp
Digital Signal Processor	DSP
Transfer Function	TF
Electromagnetic Force	E.M.F.
Discrete Technology & Production Automation	DTPA
Linear Quadratic Regulator	LQR
Zero Order Holder	ZOH
Single-Input/Multiple-Output	SIMO

Pendulum-Cart System

Symbol	*Explanation*	*Units*
L	Length of the pendulum	$[m]$
l	Distance between pivot of the pendulum to the centre of mass	$[m]$
x	Displacement of the cart from the track centre	$[m]$
$\dot{x}$	Velocity of the cart	$[m/s]$
$\ddot{x}$	Acceleration of the cart	$[m/s]$
θ	Angular displacement of the pendulum from the equilibrium point	$[rad]$
$\dot{\theta}$	Angular velocity of the pendulum	$[rad/s]$
$\ddot{\theta}$	Angular acceleration of the pendulum	$[rad/s^2]$
m	Mass of the pendulum	$[kg]$
M	Mass of the cart	$[kg]$
I_p	Pendulum moment of inertia	$[kg \times m^2]$
g	Gravitational constant	$[m/s^2]$
$T^*(q, \dot{q})$	Kinetic energy	$[J]$
$V(q)$	Potential energy	$[J]$
F_{cart}	Force acting on the cart	$[N]$
b	Coefficient of friction of the rail	$[N \times s/m]$
B	Coefficient of friction of the pendulum	$[N \times s/m]$

Actuator

Symbol	*Explanation*	*Units*
$v(t);\ V$	Input voltage	$[V]$
R	Resistance of the armature	$[\Omega]$
I_{Nom}	Nominal Current of the armature	$[A]$
I	Input Current	$[A]$
L	Inductance of the armature winding	$[H]$
e	Back electromagnetic force	$[V]$
τ_m	Electromechanical Torque generated by the DC Servo Motor	$[N \times m]$
τ_L	Load Torque	$[N \times m]$
τ_{Nom}	Nominal Torque of the DC Servo Motor	$[N \times m]$
k_T	Proportionality torque constant	$[N \times m/A]$
k_e	Proportionality speed constant	$[V \times s/rad]$
k_g	Gearing Ratio	$[-]$
k_F	Proportionality force-current constant	$[A/N]$
ω_m	Angular speed of the motor shaft	$[rad/s]$
θ_m	Motor Angle	$[rad]$
ω_{Nom}	Nominal Angular speed	$[rad/s]$
J	Total effective mass moment of inertia of the flywheel, shaft, armature of the DC motor and generator	$[kg \times m^2]$
B_m	Effective viscous damping of the bearing	$[N/m \times s/rad]$
F	Force applied on the cart	$[N]$
$\frac{d\omega_m}{dt}$	Angular acceleration of the shaft	$[m/s]$
t	Mechanical time constant	$[s]$
T	Time constant	$[s]$
G_1	Gain of the DC motor	$[-]$
k	Input to force gain	$[N/V]$
r_m	Pulley radius	$[m]$

Introduction

1.1 Project Background

The inverted pendulum (IP) stabilization is one of the classical book problems which provides the stepping stone for many Systems and Control theory applications due to its theoretical value. The Segway, Metronome, Rocket Propeller, Hover Board riding and the Self-Balancing Robot are a few examples of its use. During childhood, each of us had at least once tried to equilibrate a broom on the palm, just like when a clown tries to equilibrate various objects on the top of his nose or head. Numerous research papers were written based on the analysis of Control methods for this exact problem. Due to complex characteristics and control laws needed to stabilize non-linear systems, the IP is used as a benchmark for other robust stabilization settings.

By using the underlying principles of subjects such as: Signals and Systems, Control Engineering, Mechatronics and Digital and Hybrid Control Systems the goal of stabilizing the Closed-Loop system will be obtained. Keeping the pendulum in the upright as well as central cart position with the use of feedback while applying disturbance is the goal of the project. As in most of the papers, factors such as friction, actuator modelling and limitations are not considered; this paper will provide an inclusion and analysis of the effect of these factors over the IP problem. The modelling of the system, friction account, controller design as well as maintenance of the central and vertical position, represent the four most challenging problems of this research which will constitute the main points of analysis.

The research delivers conceptual design, simulation and real-life validation of the model. Chapter 1 after a short introduction of the inverted pendulum problem, defines the state of the art, the research problem & goal. Furthermore, the system description and embedding of components is contained in Chapter 2. Describing components in the most detailed way possible is crucial in order to achieve the expected results. Hence, Chapter 3, introduces the research methodologies such as mathematical modelling and the identification of unknown variables and parameters such as friction, and dimensions estimation. As the LQR method is applied in this research, the theory, controller design, simulations and underlying methods of application are exemplified in Chapter 4. The validation of the applied control techniques can be found in Chapter 5 and finally the conclusion of the report is drawn in Chapter 6 which also treats future points for improvement.

1.2 Problem Statement

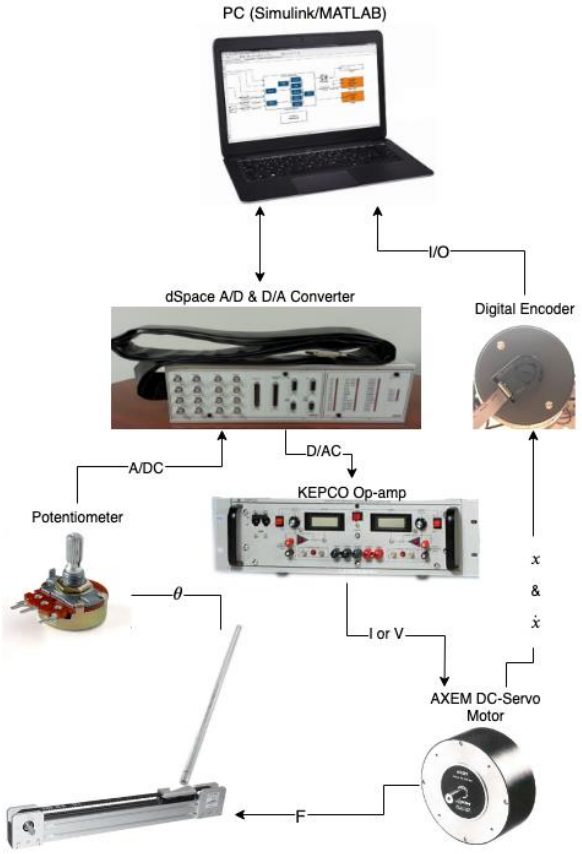

Figure 1: Current System

The problem of this project is to maintain the pendulum in an upright position by following the reference inputs while applying disturbance. The control of the pendulum-cart system will occur solely by connecting the individual components together to achieve the desired upward position. An overview of the system is provided in Figure 1. The detailed description of each component will be presented in Chapter 2.

The DC-Servo Motor is the provider of the force moving the cart which will, consequently, influence the angle of the pendulum. The motor will, in turn, be driven by the Operational Amplifier that receives the needed current/voltage based on the control law from the Simulink program. The digital transfer is converted to the real-time world through the Hardware system. Based on the feedback loop the computation of the needed input to the motor are carried out depending on the output of the system obtained using a potentiometer and encoder as the measurement devices (sensors). A more detailed description of each component will be presented in the following sections.

The system runs in real-time and the problems to be solved concern the interconnection of the subsystems which is unclear. The current research will be carried out with the idea of implementing a controller design which would stabilize the system.

1.3 Problem Owner & Stakeholder Analysis

The Inverted Pendulum was previously used by the Discrete Technology and Product Automation (DTPA) Lab Research Group at the University of Groningen [1]. Therefore, the problem owner in this situation becomes the Research Group. The outcome of the analysis will have an impact on the method they use to stabilize the IP and probably on the future problems to be solved where the IP example can be applicable. They are also the ones who would benefit from the solution.

Since the researcher Martin Stokroos worked directly with the IP and he was the first to implement the Proportional Integral (PI) double controller for the stabilization, he becomes the primary stakeholder. Moreover, as mentioned before, the Research Group of the DTPA Lab also has a stake in this project as the IP allows the use of multiple theories which can be applied to different sectors of Control Systems. As a result, by seeing the application of a different type of controller on the same inherently unstable system, the method can be applied to another setting. A possible educational demonstration can be carried out so that students from the University of Groningen understand the applicability of Control subjects better. This would potentially make students secondary stakeholders as the application of theoretical concepts in a real-life situation can make for better understanding and better use of the knowledge.

1.4 Goal & Research Questions

The goal of the thesis can be formulated as follows:

"Use the Inverted Pendulum as a test-bed for the implementation of the control theory methods taught throughout the Industrial Engineering & Management".

The main research question is:

- ⇨ *How can the individual components be characterized and connected in such a way so as to allow the control of the cart and pendulum?*

Sub Questions:

- Which unknowns are present in the system?
- What are the mathematical equations that describe the system?
- How does the actuator relate to the cart and pendulum system?
- What friction components should be included into the friction coefficient?
- Is the sampling frequency of the dSPACE hardware enough to not cause delays in the system?

These questions add to the overall knowledge of finding the answer to the main research question and once answered, the goal will be met.

1.5 Project Objectives

The goal of this research is to design a successful controller for the IP problem in order to be able to stabilize the pendulum and cart around the reference point $r_p = 0$ and $r_c = 0$. This should be done in the fastest and most accurate way which implies that the pendulum should be maintained strictly in its upward position where its rise time, settling time, steady-state value and overshoot should be optimal. The proposed goal will be attained by means of previously gained knowledge, but in order to reach it, the following sub goals must be achieved:

1. ***Identify & Obtain the relevant, unknown parameters of the system***

To be able to characterize the system in the best possible way, the parameters being used for the characterization of each component have to be defined. Experiments, literature research as well as simple measurements are going to be used for this step.

2. ***Design a suitable controller to solve 1.***

For designing a fast and accurate controller suitable for the system, theory and knowledge from the field of Control Engineering will be applied.

Some of the most relevant methods discussed and implemented in multiple research papers are the Linear Quadratic Regulator (LQR), Proportional Integral Derivative (PID), Fuzzy Logic, Sliding Mode Control (SMC) and Model Based Control (MBC). The LQR method has been chosen as the most relevant one to this research due to its extensive use as well as the assurance from its recurring use throughout many research papers. Furthermore, this method also compensates for the limitations present in approaches already taught during the course material of BSc Industrial Engineering & Management. Its working principle will be discussed at a later stage.

3. Test 2. by Simulating

The implementation of the stabilization theory on the example of the inverted pendulum will show how the chosen controller behaves. The obtained simulation and experimental results are an eminent part to the next stage of analysis and hence, are indispensable to achieve the goal set.

4. Performance comparison

As mentioned, the analysis of the experimental results is needed to see if the achievement of upright position is possible. The behaviour of the implemented controller will aid in answering the main research problem.

System Description

2.1 Scope of the System

A thorough understanding of the composite parts and unknown parameter identification must be carried out. The plant, controller, reference input, output and feedback must be specified. Based on the original setting of the experiment where all the components are interconnected, the delimitation between the Plant and the Controller was made depending on the type of equipment. The reference signals are the ones to which the Controller is comparing the actual angle and cart position.

A Digital to Analog (D/A) as well as an Analog to Digital (A/D) converter is needed for creating the connection between the real-time and discrete time system. The operational amplifier receives the needed voltage input to the motor based on the feedback law applied. The cart is affected by the motor output (angular position) which in turn, is coupled with the rail and therefore affects the location x of the cart. The position change of the pendulum angle is triggered by the cart motion as well as by a possible external disturbance $D(s)$.

There are two sensors measuring three outputs which are the pendulum's angle, the motor's angular displacement and velocity. The angle readback is an analog signal which needs to be discretized. Furthermore, the sensed signals participate in the feedback loop that is fed back to the PC and the whole procedure is repeated until the desired reference point is obtained. All of these can be visualised in Figure 2.

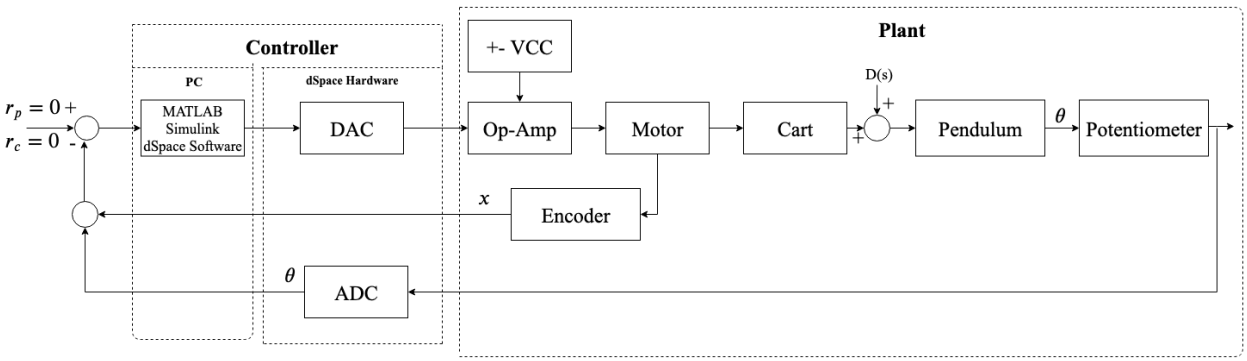

Figure 2: Block Diagram of the System

2.2 Experimental Setup

In the case of the IP there is a single input (Force applied by the DC Motor) and three outputs (Pendulum angle, Cart position and velocity). Due to the highly unstable vertical position, the problem of stabilizing the system is a challenging one. The dynamical non-linearities present in the system and its underactuated situation (one actuator and three degrees of freedom) [2], require the linearization of the model around a chosen point.

The research starts with the description of the system components followed by the state-space representation using the Euler-Lagrange mathematical modelling of the IP embedded together with the DC modelling. Currently, several unknowns are present in the setting. These must be determined by carrying out experiments and mathematical calculations. The weight and length of the cart as well as the pendulum are parameters which can be identified using a weighting system as well as approximations. Additionally, an electrical circuit for the motor to find the effect of its resistance will be designed. This resistance might affect the efficiency of the cart movement induced by the torque, depending on the input chosen. The resolution of the sensors, their importance, efficiency of the setting and holder mechanism are going to be explained and used for understanding how the system works. Other important parameters like friction will be researched and found using experiments and mathematical formulas from Physics.

2.3 Control Objective

Design a controller that makes the cart follow a specified reference trajectory for x while balancing the pendulum. The controlled system should have zero steady state error in x and adequate disturbance rejection properties (able to recover from a small tick acting the pendulum). It is worth noting that small oscillations around the reference are allowed, as these occur due to Coulomb friction as well as stiction and are difficult to overcome when using linear control only [3].

2.4 Mechanical System

The cart is driven by a toothed rubber rail which is directly coupled to a DC motor and guided by two steel bars on which the rollers of the cart slide. The pendulum is made of Aluminium where the middle of the pendulum is the centre of mass. The Cart can move along a one direction path while the pendulum can rotate in 2D along the vertical plane following a circular path due to a low friction bearing. The downward position is the equilibrium point when no force is applied, and the system is at rest. Furthermore,

the cart displacement x is represented in meters, the cart velocity $\dot{x}$ in meters per second, the pendulum angle θ in radians and the pendulum's angular velocity $\dot{\theta}$ is calculated in radians per second. The directions of the measurements conform to the ones to be described in the theoretical part of the system modelling. The respective SI units for the calculations to follow are presented in nomenclature (Pendulum & Actuator).

2.4.1 System Dynamics

To be able to control the system the states are measured constantly with the help of sensors. In this setting an encoder is used to measure the position x and speed $\dot{x}$ of the cart and a potentiometer to measure the θ angle of the pendulum. The feedback signals are decoded in the measurement subsystems which include the A/D conversion blocks and all necessary parameter calibrations. Based on the sensor readouts the driving signal (Current/Voltage) is sent to the converter which feeds the analog signal to the actuator. The gathered analog information is then transferred to the dSPACE converter for the A/D conversion with a specified sampling time T_s. The information is received by the computer (Simulink), it is then evaluated, and the control law is applied while the loop continues until the desired outcome is achieved. The PC is used in order to couple and build the control law through Simulink and MATLAB R2013b program which then runs on the dSPACE 5.2 Software.

A soft limit was set on the physical system which sets a constraint on cart position and is thus, restricted in the range of $[-0.5,0.5]$ m. This step was done to make sure that a safe experimental setup is installed where in case of an unstable implementation of the controller and unpredicted behaviour of the system, the limit cuts off any input to the motor. The Switching logic circuit can be seen in Figure 3 where based on the position of the cart, the on/off switch for power supply is triggered.

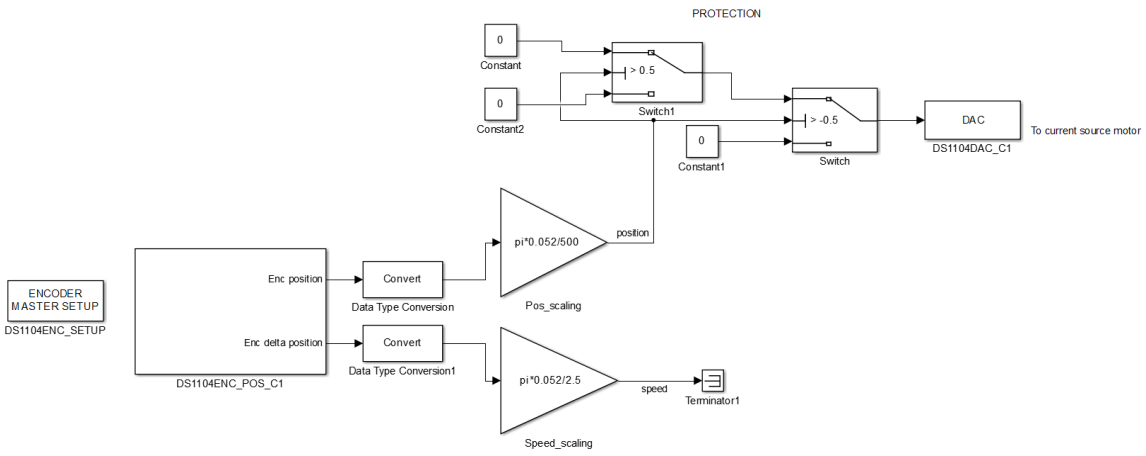

Figure 3: Cart Switching Logic Circuit

2.4.2 Controller Board/Converter

For the conversion between the digital and analog world, a Digital Signal Processor (DSP) is available. Previously, for the same purpose of control, a Simulink Target Machine (STM) microcontroller was used. The difference between them is the speed of processing data, where the DSP is much more powerful as it is faster in computing integer math and floating-point operations.

The chosen DSP for this system is the dSPACE CLP1104 Connector Panel for DS1104 R&D Controller Board which has 8 A/DC Inputs ($4\ Multiplex\ \times 16-bit;\ 4\times 12-bit$) and 8 D/AC Outputs ($16-bit$). The data acquisition and processing stage is the one the converter undertakes. The Simulink linked with the dSPACE Controller Board Software are both used for controller implementation as well as signal processing. Simulink acts as a cross-compiler by embedding the controller connected to the components, managing and calibrating the feedback signal and implementing the chosen controller to run on the DSP. The converter through which the digital system interacts with the physical one has a readout 10 times lower than the actual one which should be accounted for in the calibration step of the potentiometer readout, as it is the only sensor measurement which needs to be discretized after acquisition.

2.4.3 Power Amplifier

The KEPCO BOP 36-12M Bipolar Operational Power Supply/Amplifier can act as a Voltage or Current source for the appliance connected to it. In this research both possibilities were analysed and compared based on the efficiency with which the motor works. The saturation of the op-amp is given as $\pm 36\ V$ and $\pm 12\ A$. The fixed closed-loop gain of the operational amplifier if current is the input to be fed to the motor is $0.8333\ \frac{V}{A}$ since for each $10\ V$ fed, $12\ A$ are generated. A similar reasoning is applied for the voltage being supplied to the motor. For each $10\ V$ given to the power amplifier an output of $36\ V$ is obtained which means that a conversion factor of $0.2777\frac{V}{V}$ is used. The characteristics of the KEPCO BOP 36-12M Op-amp makes it easier to find the voltage input needed to obtain a desired force. Moreover, the scaling factor for the readback A/D current translation is $12\ \frac{A}{V}$ while for voltage it is $36\ \frac{V}{V}$ [14]. The amplified conversion for the readback signal is also caused due to the discretization step taken by the A/D converter as for the potentiometer readout.

Furthermore, the op-amp adjusts the $\pm Vcc\ (230\ V)$ Supply Voltage to fit the desired signal to be fed to the motor. The op-amp voltage and current wires are connected to two of the $12-bit$ A/D inputs for the readback and constant measuring in the dSPACE

Hardware. Similarly, the port through which the controller drives the op-amp is connected to one of the $12-bit$ D/A inputs of the controller board.

2.4.4 Sensors

2.4.4.1 Encoder

The encoder used in this setting is the Quick Assembly Two Channel Optical Quadrature Encoder **HEDL-5540-A12** by Avago Technologies characterized by high reliability and high resolution. A standard resolution of up to $N = 500\ cycles\ per\ revolution$ is available for the aforementioned encoder [24]. A more detailed explanation of the working principle of the encoder, the conversion possibilities and the equation deduction for the measurement outputs can be found in Appendix IIIa. Thus, based on equation (C) & (D) from Appendix IIIa the scaling factors for the position and speed are as follows:

$$Position\ Gain = 0.000327 \frac{m}{pulse}$$

$$Velocity\ Gain = 0.0654 \frac{m}{s \times pulse}$$

2.4.4.2 Potentiometer

The potentiometer is the sensor used to find the angle of the pendulum. It is attached to the pivot point between the cart and the pendulum. By measuring the distance or displacement of an object in a linear or rotary motion it converts the value into an electrical signal. The pendulum is connected directly to the rotational shaft of the potentiometer and a DC reference voltage is applied across the two outer fixed connections forming the resistive element. The signal attained from the physical element is then converted by the A/D Converter. As such, the difference between the reference signal and the potentiometer output facilitates the control signals that drives the system. The detailed working principle of the potentiometer together with its specifications can be found in Appendix IIIb. Based on equation eq. (L) from Appendix IIIb the scaling factor to consider for the ADC angle θ conversion for the potentiometer measurement is given as:

$$Resolution = 0.314 \frac{rad}{V}$$

Due to the fact that the potentiometer does not offer the angular velocity measurement, a discrete time derivative was used in order to obtain the measurement of the $\dot{\theta}$ state as seen in Figure 27 from Appendix IIIb.

2.4.5 Actuator

The actuator used in the presented setting is the AXEM/CEM F9M4 Serie F Type of DC Servo Motor. The principle of a DC motor is to convert electrical energy to mechanical motion. The mechanism drives the conveyor belt and hence; the cart. The motor applies a certain torque generated by the connection to the operational amplifier and the control law running on the DSP. This rotational movement translates to a linear translational one, which is the force driving the cart [4]. The cart is driven by the DC motor according to the control current or voltage law. As soon as the threshold of $[-0.5; 0.5]$ m is reached, the input to the motor will be 0. The approximate calculation of the shaft radius connected to the toothed rail which drives the cart was carried out in Appendix IV.

Research Methodology

3.1 System Representation

The dynamics of the system can be written down and derived using Newton's 2nd Law of Motion or Euler-Lagrange Modelling. As mentioned before, there are two degrees of freedom which will help in defining the states of the system. Those are the Cart Position and Pendulum Angle.

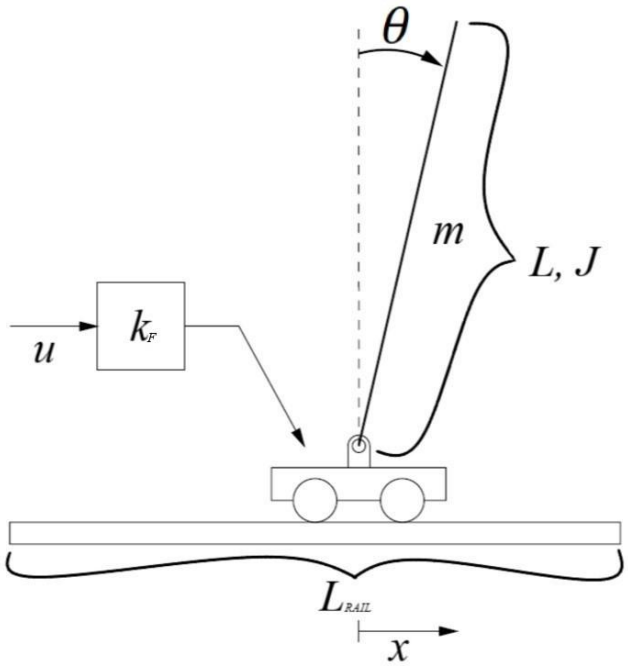

Figure 4: Inverted pendulum System Component [3]

Figure 4 shows the components that interact with the pendulum. The system consists of a cart with mass M and location x, a pendulum with mass m situated at an inclined angle θ from the vertical axis, an input force u sent to the DC Motor as current or voltage converted to force acting on the cart.

3.2 Mathematical Modelling

Measuring the dimensions and masses provides data sets which are important to carry out further calculations that will be carried out in subsequent sections. It is assumed that the hinge which connects the pendulum with the cart is frictionless (low-friction

pivot), thus $B = 0$ [15]. Furthermore, the friction between the pendulum and the pivot is much smaller than that between the cart and the rail, and thus, is neglected [16].

To find the Dynamical Model of the system, the position of the pendulum as well as the cart must be identified:

Pendulum:	*Cart:*
$x_p = x + \frac{L}{2}\sin(\theta)$	$x_c = x$
$y_p = \frac{L}{2}\cos(\theta)$	$y_c = 0$

Where $L = 2 \cdot l$

The velocity can be written as the change in position by applying the Pythagoras Trigonometric Identity:

$$v_p^2 = x_p^2 + y_p^2 \tag{1}$$

$$v_c^2 = x_c^2 + y_c^2 \tag{2}$$

Euler-Lagrange Equation:

$$\frac{d}{dt}\frac{\partial \mathcal{L}}{\partial \dot{q}} - \frac{\partial \mathcal{L}}{\partial q} = F^d + F^e \tag{3}$$

Where $\mathcal{L}$ is the Lagrangian, q and $\dot{q}$ are the states of the system, F^d is the damping force expressed by the Rayleigh dissipation function as $-\frac{dD}{d\dot{q}}$, and F^e is the external force expressed by Bu.

The LaGrangian is represented by:

$$\mathcal{L} = T^*(q, \dot{q}) - V(q) \tag{4}$$

where $T^*(q, \dot{q})$ is the Total Kinetic Energy (KE) and $V(q)$is the Total Potential Energy (PE).

$T^*(q, \dot{q})$ is composed of the Mechanical Translational component of both the cart and the pendulum $\frac{1}{2}Mv_c^2 + \frac{1}{2}mv_p^2$ and the Mechanical Rotational component $\frac{1}{2}I_p\dot{\theta}^2$.

$$T^*(q,\dot{q}) = \frac{1}{2}Mv_c^2 + \frac{1}{2}mv_p^2 + \frac{1}{2}I_p\dot{\theta}^2 \tag{5}$$

I_p is the Pendulum's Moment of Inertia [32] about the pivot to the its centre of Gravity/Mass expressed as:

$$I_p = \frac{1}{3}ml^2 = \frac{1}{12}mL^2 \tag{6}$$

$$V(q) = mgh = mgy_p = mgl\cos(\theta) \tag{7}$$

By substituting eq. (5) & (7) into (4) and solving for the values of $(x,y)_{p,c}$ the following is obtained:

$$\mathcal{L} = \frac{1}{2}(M+m)\dot{x}^2 + ml\dot{x}\dot{\theta}\cos\theta + \left(\frac{1}{2}I_p + \frac{1}{2}ml^2\right)\dot{\theta}^2 - mgl\cos\theta \tag{8}$$

Differentiation:

x	θ
$\frac{\partial\mathcal{L}}{\partial x} = 0$	$\frac{\partial\mathcal{L}}{\partial\theta} = -ml\dot{x}\dot{\theta}\sin\theta + mgl\sin\theta$
$\frac{\partial\mathcal{L}}{\partial\dot{x}} = (M+m)\dot{x} + ml\dot{\theta}\cos\theta$	$\frac{\partial\mathcal{L}}{\partial\dot{\theta}} = ml\dot{x}\cos\theta + \left(I_p + ml^2\right)\dot{\theta}$
$\frac{d}{dt}\frac{\partial\mathcal{L}}{\partial\dot{x}} = (M+m)\ddot{x} - ml\dot{\theta}^2\sin\theta + ml\ddot{\theta}\cos\theta$	$\frac{d}{dt}\frac{\partial\mathcal{L}}{\partial\dot{\theta}} = ml\ddot{x}\cos\theta - ml\dot{x}\dot{\theta}\sin\theta + \left(I_p + ml^2\right)\ddot{\theta}$

Combining into eq. (3) gives:

$$(M+m)\ddot{x} - ml\dot{\theta}^2\sin\theta + ml\ddot{\theta}\cos\theta = F_{cart} - b\dot{x} \tag{9}$$

$$ml\ddot{x}\cos\theta + \left(I_p + ml^2\right)\ddot{\theta} - mgl\sin\theta = 0 \tag{10}$$

Hereby the non-linear equations are obtained. By using Taylor Series small-angle approximation $sin\,\theta \approx \theta$, the non-linear set of equations are linearized. The stabilization of the pendulum's angle must be done at the inverted position.

Assuming:

$$\theta \approx 0$$

$$\sin\theta \approx \theta$$

$$\cos\theta \approx 1$$

$$\dot{\theta}^2 \approx 0$$

The system's equations become:

$$(M+m)\ddot{x} + ml\ddot{\theta} = F_{cart} - b\dot{x} \tag{11}$$

$$\left(I_p + ml^2\right)\ddot{\theta} + ml\ddot{x} - mgl\theta = 0 \tag{12}$$

Substituting $\ddot{\theta}$ from eq. (11) with the one from eq. (12) the following equation is obtained:

$$\ddot{x} = \frac{1}{(M+m)p}F_{cart} - \frac{b}{(M+m)p}\dot{x} - \frac{(ml)^2 g}{(M+m)\left(I_p + ml^2\right)}\theta \tag{13}$$

Where $p = 1 - \frac{(ml)^2}{(M+m)\left(I_p+ml^2\right)}$.

Similarly, the same can be done to $\ddot{x}$ from eq. (12) by substituting the one from eq. (11):

$$\ddot{\theta} = \frac{mlg}{\left(I_p + ml^2\right)p}\theta + \frac{bml}{(M+m)\left(I_p + ml^2\right)p}\dot{x} - \frac{ml}{(M+m)\left(I_p + ml^2\right)p}F_{cart} \tag{14}$$

3.3 Circuit analysis

The rotational direction of the DC servo motor depends on the sign of the Current/Voltage which controls the pendulum by moving the cart backward or forward. This section tackles the current controlling part of the circuit [6]. The Analog controller receives the angle and cart position and based on that it controls the servomotor, ensuring continuous and consistent traction [7]. Table 1 presents the physical characteristics of the DC Servo Motor relevant to the exact model type as mentioned above (Document provided by CEM, renamed as AXEM).

	Symboles Symbols		F 9 M 4 Fermé Uncooled	
1 - MOTOR RATINGS (1)				
Rated torque	Cn	N.cm	34,6	
Rated speed	Nn	tr/min r.p.m.	3000	
Rated output (2)	Pn	W	108	
Rated voltage	Un	V	26	
Rated current	In	A	6,7	
Maximum at very low speed*	Icc	A	6,7	
Pulse torque (intermittent operation) (3)	Cimp	N.cm	345	
Maximum speed with no external load**	Nmax	tr/min r.p.m.	8000	
* Stall motor : ask us for max. current ** For other duty cycles : ask us				
2 - MOTOR CONSTANTS				
E.M.F. / 1 000 r.p.m.	K_E	V	6,2	
Torque constant / ampère	K_T	N.cm	5,92	
Régulation constant voltage / N.cm	K_N	tr/min r.p.m.	29,3	
Friction torque	T_f	N.cm	2,5	
Damping constant / 1 000 r.p.m.	K_D	N.cm	0,8	
Terminal resistance (4)	R	Ω	1,10	
Armature inductance	L	μH	< 100	
Total inertia	J	g.cm²	350	
Mechanical time constant	τ	ms	10,2	
Power rate (5)	Ps	kw/s	340	

Table 1: DC motor Characteristics

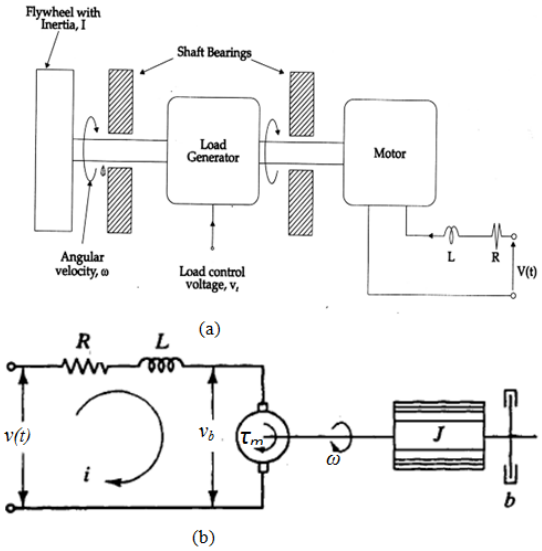

Figure 5: Simplified schematic diagram of DC motor and accessories [10].

The Motor has both a back-emf constant as well as a torque constant. Since there is a possibility of either using only the torque constant or both, the analysis of both cases was carried out. The values of the torque constant k_T and the one of the back-emf constant k_e correspond in SI: $k_T\left(\frac{Nm}{A}\right) = k_e\left(\frac{Vs}{rad}\right)$ which is true if $\frac{V}{RPM}$ is transformed to $\frac{Vs}{rad}$, the same k_T is obtained:

$$\frac{Rev}{min}\frac{min}{60\ sec}\frac{2\pi\ rad}{1} = \frac{rad}{sec} \tag{15}$$

Thus, either just one of the constants or both can be used in the calculations.

3.3.1 Current Input Modelling

Since the motor can be driven by a current operational amplifier besides the voltage one, the equations needed to express the relationship between the coupling will change. For this case the back-emf as well as the motor resistance should not be considered due to constant current [13]. As a result, the torque constant k_T allows to express the relationship between the force and the input current by using the force-current gain k_F.

Hence, the torque created by the motor is directly coupled to the current applied to the motor, which, can be extended to describe the applied force on the cart and the current coming from the controller. As shown in Figure 30 from Appendix IIIc, the cart and the motor are connected directly through the pulley and the toothed belt. Thus, the

coupling equation is given by the external load torque which is equal to the electromechanical torque from Appendix IV.

$$r_m F = k_T k_g I \tag{16}$$

Where k_F is:

$$k_F = \frac{r_m}{k_T k_g} = \frac{0.026\ m}{0.0592 \frac{Nm}{A}} = 0.4392 \frac{A}{N} \tag{17}$$

Since, the belt used for this setting is toothed and has been manufactured for such situations; the assumption that the belt is non-elastic and no-slipping was made.[51].

The input-to-force gain k_F can also be calculated by carrying out the experiment where a constant ramp current input is fed to the motor which will translate it into a force that can be found with the help of a strain gauge once the cart is restrained from moving.

$$I = k_F F \tag{18}$$

The k_F will therefore be found by dividing the Current by pulling Force.

$$F_h + m\ddot{x} + b\dot{x} = F \tag{19}$$

Hereby, by not having any displacement, speed or acceleration the force with which the cart is restrained from moving (human force) is equal to the force with which the motor wants to move the cart to a certain direction. Therefore, the strain gauge reads the value for the force which can then be compared to the actual value based on the conversion factor.

Current Fed $[A]$	*Actual Force* $[N]$			*Expected Force* $[N]$	k_F	
	I Trial	*II Trail*	*Average*		*Actual*	*Expected*
1 A	0	0	0	2.276867031	0	0.4392
2 A	0	0	0	4.553734062	0	0.4392
3 A	2	2.15	2.075	6.830601093	1.445783133	0.4392
4 A	2.5	3.3	2.9	9.107468124	1.379310345	0.4392
5 A	5	5.75	5.375	11.38433515	0.930232558	0.4392
6 A	6.8	7.5	7.15	13.66120219	0.839160839	0.4392
7 A	8	8.95	8.475	15.93806922	0.825958702	0.4392
8 A	11	10.9	10.95	18.21493625	0.730593607	0.4392
9 A	12.5	13.3	12.9	20.49180328	0.697674419	0.4392

10 A	16	15.5	15.75	22.76867031	0.634920635	0.4392
11 A	17.5	17.4	17.45	25.04553734	0.630372493	0.4392
12 A	20	21	20.5	27.32240437	0.585365854	0.4392

Table 2: Data for Comparison from the Strain Gauge Experiment

The measurements were taken three times in order to make sure that the experimental data is accurate. As observed in Table 2, the actual force differs from the one expected. This implies that the conversion factor (force-current gain) is different in practice. Similarly, a so called "dead zone" for the current input exists, for which the cart does not encounter any movement due to the static friction present between the rail and the cart.

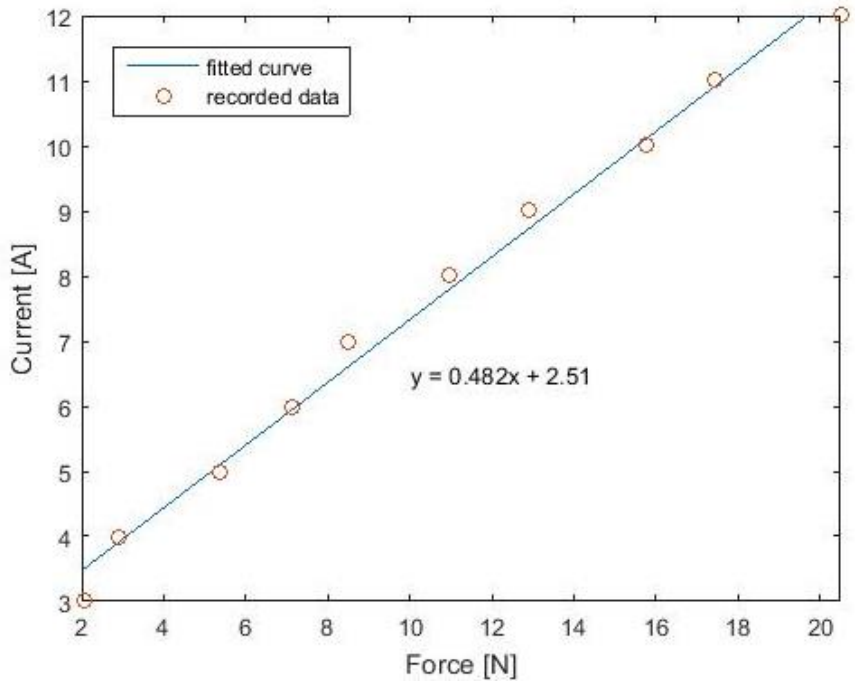

Figure 6: Current to Force experiment line fit

Thus, the equation of the coupling is given by the gathered data as seen in Figure 6:

$$I = 0.482F + 2.51 \tag{20}$$

The MATLAB code needed to generate Figure 6 and for the relationship equation of the line can be found in Appendix Ic.

The presence of the static friction coefficient can already be detected due to the fact that the strain gauge reading starts from 3 *Amperes* onwards, thus the cart does not move until the motor input current does not reach $\sim 3\ A$. Once the friction factor is

considered, the error between the actual and expected force reading is anticipated to decrease considerably so as to be able to use the predicted force-current gain k_F.

Equation (20) confirms that indeed, the expected force to current coefficient $k_{Fexpected} = 0.4392$ is very close to the actual one $k_{Factual} = 0.482$ once the static friction impact is considered.

It is worth mentioning that, small errors due to inaccurate reading as well as external disturbances are not uncommon.

Thus, for the Current driven DC motor, the force to current gain which will be used in the simulations and experiments is given by eq. (20).

3.3.2 Voltage Input Modelling

For the calculation of the voltage modelling, there are two possibilities, the time and frequency domain. As the equations used for deriving the interconnection between voltage and force are generally used and known, the extensive steps for calculating the relation can be found in Appendix IV. Thus, the relationship between force and voltage is given by eq. (A6) from Appendix IVb as:

$$F = \frac{k_T k_g}{r_m R} V - \left(\frac{k_T k_g^2 k_e}{r_m^2 R} + \frac{B k_g}{r_m^2} \right) \dot{x} - \frac{J k_g}{r_m^2} \ddot{x}$$

Substituting F from eq. (A6) into eq. (13) and (14) results in:

$$\ddot{x} = \frac{1}{(M+m)p} \frac{k_T k_g}{r_m R Z} V - \frac{1}{(M+m)pZ} \left(\frac{B k_g}{r_m^2} + \frac{k_T k_g^2 k_e}{r_m^2 R} + b \right) \dot{x} - \frac{(ml)^2 g}{(M+m)\left(I_p + ml^2\right) Z} \theta \qquad (22)$$

With $Z = 1 + \frac{J k_g}{r_m^2 (M+m) p}$ and

$$\ddot{\theta} = \frac{ml}{\left(I_p + ml^2\right)(M+m)p} \left(\frac{B k_g}{r_m^2} + \frac{k_T k_g^2 k_e}{r_m^2 R} + b \right) \dot{x} + \left(\frac{mlg}{\left(I_p + ml^2\right)} + \frac{(ml)^3 g}{\left(I_p + ml^2\right)^2 (M+m) Z} \right) \theta -$$

$$- \frac{ml}{\left(I_p + ml^2\right)(M+m)p} \frac{k_T k_g}{r_m R Z} V \qquad (23)$$

3.4 State Space Model

As a follow up to the mathematical modelling section, the state space representation is carried out.

3.4.1 Current input State-Space

$$\begin{bmatrix} x_1 \\ x_2 \\ x_3 \\ x_4 \end{bmatrix} = \begin{bmatrix} x \\ \dot{x} \\ \theta \\ \dot{\theta} \end{bmatrix} \tag{24}$$

$$\begin{bmatrix} \dot{x}_1 \\ \dot{x}_2 \\ \dot{x}_3 \\ \dot{x}_4 \end{bmatrix} = \begin{bmatrix} \dot{x} \\ \ddot{x} \\ \dot{\theta} \\ \ddot{\theta} \end{bmatrix} \tag{25}$$

Where the dummy states are given by $\dot{x_1} = x_2$ and $\dot{x_3} = x_4$.

Based on eq. (13) and eq. (14), the matrix form is represented as:

$$\begin{bmatrix} \dot{x}_1 \\ \dot{x}_2 \\ \dot{x}_3 \\ \dot{x}_4 \end{bmatrix} = \begin{bmatrix} 0 & 1 & 0 & 0 \\ 0 & -\frac{b}{(M+m)p} & -\frac{(ml)^2 g}{(M+m)(I_p+ml^2)p} & 0 \\ 0 & 0 & 0 & 1 \\ 0 & \frac{bml}{(M+m)(I_p+ml^2)p} & \frac{mlg}{(I_p+ml^2)p} & 0 \end{bmatrix} \begin{bmatrix} x_1 \\ x_2 \\ x_3 \\ x_4 \end{bmatrix} + \begin{bmatrix} 0 \\ \frac{1}{(M+m)p} \\ 0 \\ -\frac{ml}{(M+m)(I_p+ml^2)p} \end{bmatrix} F \tag{26}$$

$$y = \begin{bmatrix} 1 & 0 & 0 & 0 \\ 0 & 0 & 1 & 0 \end{bmatrix} \begin{bmatrix} x_1 \\ x_2 \\ x_3 \\ x_4 \end{bmatrix} + \begin{bmatrix} 0 \\ 0 \end{bmatrix} \tag{27}$$

Where based on eq. (20) $I = 0.482F + 2.51$.

3.4.2 Voltage input State-Space

Similarly, based on eq. (22) and eq. (23), the matrix form, for the Voltage driven DC-Motor, is as follows:

$$\begin{bmatrix}\dot{x}_1\\ \dot{x}_2\\ \dot{x}_3\\ \dot{x}_4\end{bmatrix} = \begin{bmatrix}0 & 1 & 0 & 0\\ 0 & -\frac{1}{(M+m)pZ}\left(\frac{Bk_g}{r_m^2}+\frac{k_T k_g^2 k_e}{r_m^2 R}+b\right) & -\frac{(ml)^2 g}{(M+m)\left(I_p+ml^2\right)Z} & 0\\ 0 & 0 & 0 & 1\\ 0 & \frac{ml\left(\frac{Bk_g}{r_m^2}+\frac{k_T k_g^2 k_e}{r_m^2 R}+b\right)}{\left(I_p+ml^2\right)(M+m)p} & \left(\frac{mlg}{\left(I_p+ml^2\right)}+\frac{(ml)^3 g}{\left(I_p+ml^2\right)^2(M+m)Z}\right) & 0\end{bmatrix}\begin{bmatrix}x_1\\ x_2\\ x_3\\ x_4\end{bmatrix} +$$

$$+\begin{bmatrix}0\\ \frac{1}{(M+m)p}\frac{k_T k_g}{r_m RZ}\\ 0\\ -\frac{mlk_T k_g}{\left(I_p+ml^2\right)(M+m)pr_m RZ}\end{bmatrix}V \tag{28}$$

$$y = \begin{bmatrix}1 & 0 & 0 & 0\\ 0 & 0 & 1 & 0\end{bmatrix}\begin{bmatrix}x_1\\ x_2\\ x_3\\ x_4\end{bmatrix} + \begin{bmatrix}0\\ 0\end{bmatrix} \tag{29}$$

3.5 Parameter Identification

3.5.1 Dimension and Weight Calculation

Cart

An approximation of the cart mass was made since its full disassembling was not possible. The total mass of the cart is $1303.2\ g = 1.3032\ kg$. A more detailed explanation of the calculation method is presented in Appendix VIII.

Pendulum

The mass of the pendulum was determined with the help of a scale $m = 0.277\ kg$ and a ruler was used to identify the length $L = 0.868\ m$ of the pendulum.

3.5.2 Discretization

A digital controller for a continuous-time plant is often designed in order to find the discrete time equivalent of a continuous system. Since the controller used in the research is digital and implemented on a PC, the conversion of the system must be computed which, will also help in foreseeing the behaviour of the system during simulations, how the system will behave. Thus, the continuous state-space model will be first discretized by using the Zero order holder (ZOH) method of continuous time discretization. The ZOH transformation is a design of discrete equivalents via holding

each sample value for one sample interval. The sampling period chosen for this setup is 200 Hz or 5 ms as the sampling should not be too high so that no small changes are encountered in measured data each step, otherwise this will lead to a greater amount of unnecessary data to be processed. The sampling period is also set to be high enough to produce negligible phase loss at crossover [11]. It will be later shown that due to this step, the outcome of the derivative states will be characterized by counting errors and thus spikes.

3.5.3 Friction Identification

Friction is defined as the force resisting the relative motion of solid surfaces, fluid layers, and material elements sliding against each other [38]. It is one of the most important components of the mechanical equipment that is non-linear and has a direct impact on the behaviour of the system where some of the undesirable effects are steady-state error, limit cycles and hunting. The classic control theory is based on linearity and feedback is not able to fully compensate for frictional effects. By assuming no other non-linearities are present in the system, the friction component can be accounted for and removed from the picture [39]. Major contributors to the friction in the IP are the Pulley-Toothed Rail-Cart system and the DC Servo Motor. The current/voltage that comes from the power amplifier is converted to torque generated by the motor which then translated to force that acts on the cart.

There are generally three friction components present in a system: Viscous, Coulomb and Static (Dry). These influence the performance of the system and should be considered to account for the interference. The linear nature of Coulomb and viscous friction models makes them an attractive choice for many engineering problems. Often, the simple linear viscous friction will be enough to characterize the friction factor [22, 45]. This is due to the fact that the Coulomb and Static friction components contribute little to the total friction component while the Viscous becomes the dominant friction force for the model [40]. Furthermore, as it is harder to model the Coulomb friction, it is possible to incorporate its effects straight into the control by making the friction coefficient “more positive” [41].

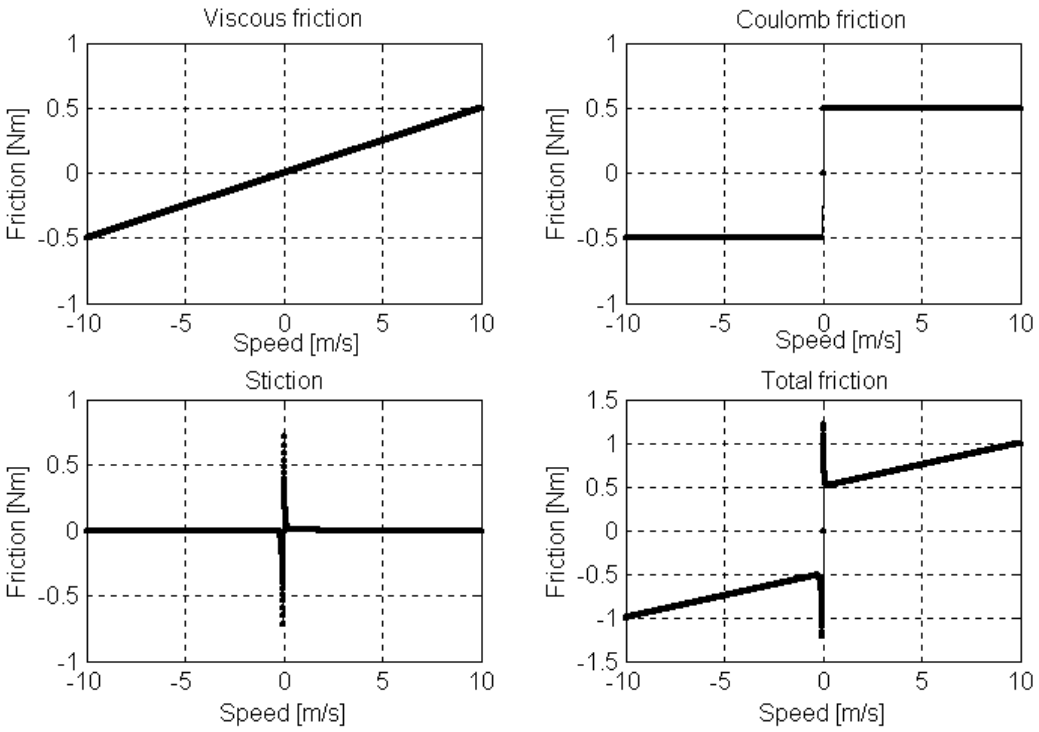

Figure 7: Representations of friction models: viscous, Coulomb, Static and mixed [26].

As can be seen in Figure 7, the total friction behaves in a nonlinear way, and this will lead to complex structures of the friction model.

In [16] the author mentions that the controller designed only by using viscous friction has poor performance. The equations for the friction model are presented and the resulting model is then complex due to presence of non-linearities.

$$F_f = \begin{cases} F_s & if\dot{x} = 0 \\ F_c + F_v & if\dot{x} \neq 0 \end{cases} \tag{30}$$

Eq. (30) represent the total friction force [16].

Friction Type	**Dependence**	**Formula**
Coulomb (kinetic)	Dependent on velocity and proportional to normal load.	$F_c = -\mu_c F_N sgn(\dot{x})$ (31)
Viscous	Arises in lubricated systems, is proportional to velocity and goes to zero when motion stops.	$F_v = -\varepsilon\dot{x}$ (32)

Static	Friction force at zero velocity, prevents slipping, known to be greater than kinetic fiction and is modelled as proportional to normal load.	$F_s = \begin{cases} -F & if\ \lvert F\rvert < \mu_s F_N \\ -\mu_s F_N sgn(F) & if\ \lvert F\rvert \geq \mu_s F_N \end{cases}$ (33)

Table 3: Friction type dependence

The system has several components which contribute the most to the friction coefficient, namely:

- ➔ The Cart Rollers: Steel on Aluminium Coefficient [46], $\mu_c = 0.47$, $\mu_s = 0.61$
- ➔ The Toothed Belt on Bearing: Rubber on Steel [47], $\mu_c = 0.475, \mu_s = 0.79$

As expected, the coefficients of static friction are higher than the Coulomb coefficients [48].

The viscous friction depends on the speed of rotation that the motor generates, and this dependence is linear. The Coulomb force depends on the type of materials that touch as well as the thrust force between them. Moreover, static friction is present between the stationary object and the surface on which it is resting, and it prevents the object from moving against a surface. Thus, whenever the object wants to move the static friction is the first to overcome. Simple tests with the motor-cart system show that friction forces have a nonlinear nature [26].

By taking [43] as an example, the values for static, Coulomb and viscous friction can be found through several experiments.

3.5.3.1 Coulomb and Viscous friction

For this experiment, the situation when the cart is in motion is relevant. Therefore, based on eq. (30), $F_f = F_c + F_v, when\ \dot{x} \neq 0$.

From Appendix IVb, the force is given by eq. (A6):

$$F = \frac{k_T k_g}{r_m R} V - \left(\frac{k_T k_g^2 k_e}{r_m^2 R} + \frac{B k_g}{r_m^2} \right) \dot{x} - \frac{J k_g}{r_m^2} \ddot{x}$$

Where

$$\alpha = \frac{k_T k_g}{r_m R} \quad (35)$$

$$\beta = \frac{k_T k_g^2 k_e}{r_m^2 R} + \frac{B k_g}{r_m^2} \tag{36}$$

$$\gamma = \frac{J k_g}{r_m^2} \tag{37}$$

And therefore eq. (A6) becomes:

$$F = \alpha V - \beta \dot{x} - \gamma \ddot{x} \tag{38}$$

Newton's second law tells states that when a force is applied to a mass, the mass experiences an acceleration proportional to the applied net force [49].

$$\sum F = ma = m\ddot{x} \tag{39}$$

Where a is the acceleration of the object, ΣF is the net force on the object, and m is the mass of the object.

In this system the net force is expressed as:

$$\sum F = F + F_f \tag{40}$$

Therefore:

$$m\ddot{x} = \alpha V - \beta \dot{x} - \gamma \ddot{x} + F_f \tag{41}$$

And F_f is:

$$F_f = F_c + F_v = -\mu_c F_N sgn(\dot{x}) - \varepsilon \dot{x} \tag{42}$$

As the cart moves horizontally in one direction and therefore forward, $sgn(\dot{x}) = 1$ and the normal force is given by $F_N = Mg$. Once the cart is driven by constant Voltage and runs forward on the rail with constant velocity $\dot{x}$, the acceleration will reach it's minimum $\ddot{x} = 0 \frac{m}{s^2}$ and equation (40) will become:

$$F = -F_f \tag{43}$$

Hence resulting in:

$$\alpha V - \beta \dot{x} = \mu_c F_N + \varepsilon \dot{x} \tag{44}$$

The values for the calculated parameters can be found in Table 4.

Symbol	Value	Description
R	$1.1\ \Omega$	Motor Resistance
m	$0.277\ Kg$	Pendulum mass
M	$1.3032\ Kg$	Cart mass
L	$0.868\ m$	Pendulum length
J	$3.5 \times 10^{-5}\ kg \times m^2$	Total mass moment of inertia
B	$2.3 \times 10^{-4}\ N \times m \times \frac{s}{rad}$	Effective viscous damping of the bearing
g	$9.8066 \frac{m}{s^2}$	Gravitational constant
k_T	$0.0592 \frac{N \times m}{A}$	Torque proportionality constant
k_e	$0.0592\ V \times \frac{s}{rad}$	Back-EMF constant
k_g	1	Gearbox ratio
r_m	$0.026\ m$	Motor shaft diameter
F_{N1}	$12.78\ N$	Normal Force (Cart only)
F_{N2}	$15.5\ N$	Normal Force (Cart + Pendulum)
α	$2.069\ N \times V$	$\frac{k_T k_g}{r_m R}$
β	$5.053\ N \times \frac{s}{m}$	$\frac{k_T k_g^2 k_e}{r_m^2 R} + \frac{B k_g}{r_m^2}$
γ	$0.052N \times \frac{s^2}{m}$	$\frac{J k_g}{r_m^2}$

Table 4: Known values needed for the experiments

In this situation only the cart mass was used for the experiment. Thus, the normal force is given by F_{N1}. Hence, by recording the values for Voltage input to the motor, and constant velocity a mapping of the equations can be carried out. Taking two of the recorded values of Voltage the respective velocity and solving the set of equations will give the coefficients of friction μ_c and ε. To make sure that the values are accurate, a set of 10 consecutive experiments took place where the constant velocity for each Voltage input was measured three times.

$$2.069V - 5.053\dot{x} = \mu_c 12.78 + \varepsilon\dot{x} \tag{45}$$

After carrying out the experiment, the following results were obtained:

$Nr.$	$V\ to\ motor$	$\dot{x}$
1	4.57031	0.065345
2	5.32617	0.179699
3	5.73047	0.245044
4	5.7832	0.277717
5	6.04688	0.294053
6	6.16992	0.343062
7	6.83789	0.490088
8	7.7138	0.70246
9	7.80469	0.718796
10	9.94922	1.19255

Table 5: Recorded values

Running the solver based on eq. (45) returns the values of $\mu_c = 0.722969905$ and $\varepsilon = 5.134270476\,\frac{\mathrm{Ns}}{\mathrm{m}}$.

3.5.3.2 Static friction

As given in eq. (33), static friction is the first friction force to overcome so that the cart starts to move. Thus, the situation when $\dot{x} = 0$ is analyzed.

For the experiment, the strain gauge was used. By recording the maximum force, which is required to move the cart, the coefficient of friction can be found based on the following equation:

$$\mu_s F_N = F \tag{46}$$

The experiment was repeated several times for precision. The outcome can be seen in Table 6.

Trail	Force [N]
1	9.6
2	11
3	10.5
4	9.1
5	10.2
6	9.5
Average	9.98333

Table 6: Strain Gauge Experiment

Therefore, after running the calculations, the coefficient of static friction is found as; $\mu_s = 0.7811659$. As expected, the Static friction coefficient is higher than the Coulomb one.

Thus, the Friction force for the whole system where the normal force is given by F_{N2}, can be described by:

$$F_f = \begin{cases} \begin{cases} -F & if\ |F| < 12.108 \\ -12.108sgn(F) & if\ |F| \geq 12.108 \end{cases} & if\dot{x} = 0 \\ -11.206sgn(\dot{x}) - 5.1343\dot{x} & if\dot{x} \neq 0 \end{cases} \tag{47}$$

3.5.4 Friction Validation

In order to validate that friction forces are indeed present in the system and that the relationship between force and current is indeed not a linear one, the behaviour of the system where a square pulse input is given to the motor was analysed [55].

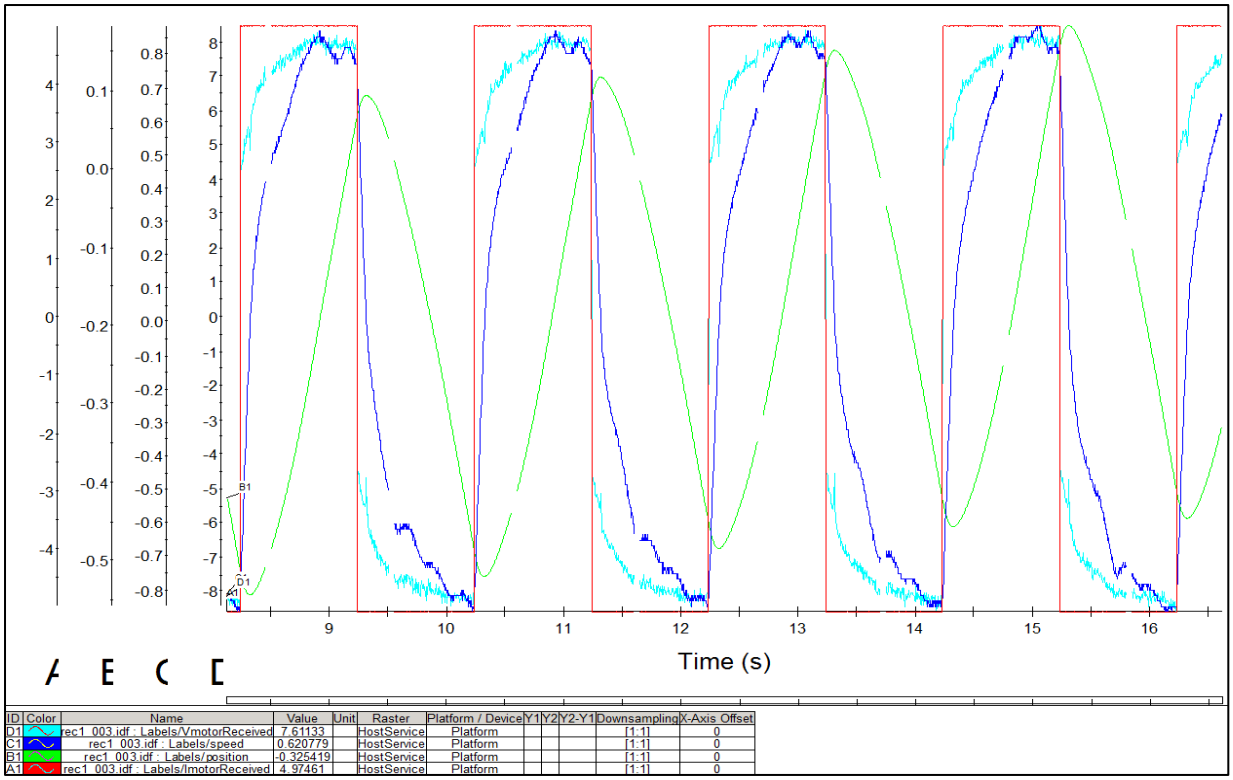

Figure 8: Current Drive Pulse Response

For the Current driven system, who's response can be seen in Figure 8, a square wave with a pulse width of 1 sec and a 5 *A* amplitude has been fed to the motor. What can be deduced from the graph is that the motor response is slower than the input value, and therefore, there is a delay in the system. Furthermore, the presence of noise in the encoder cart velocity reading has been detected, which is due to the discretization of the signal. As visualized, the cart velocity cannot follow the pulse precisely, which might be caused by the friction forces as well as by the inertia that the motor has to drive. To start following the input signal, a delay of 0.68 sec was recorded. Furthermore, it can be clearly seen that the friction throughout the rail length is not linear, by analysing the spikes in velocity readout, which will lead to a different behaviour of the systems when compared to the simulations.

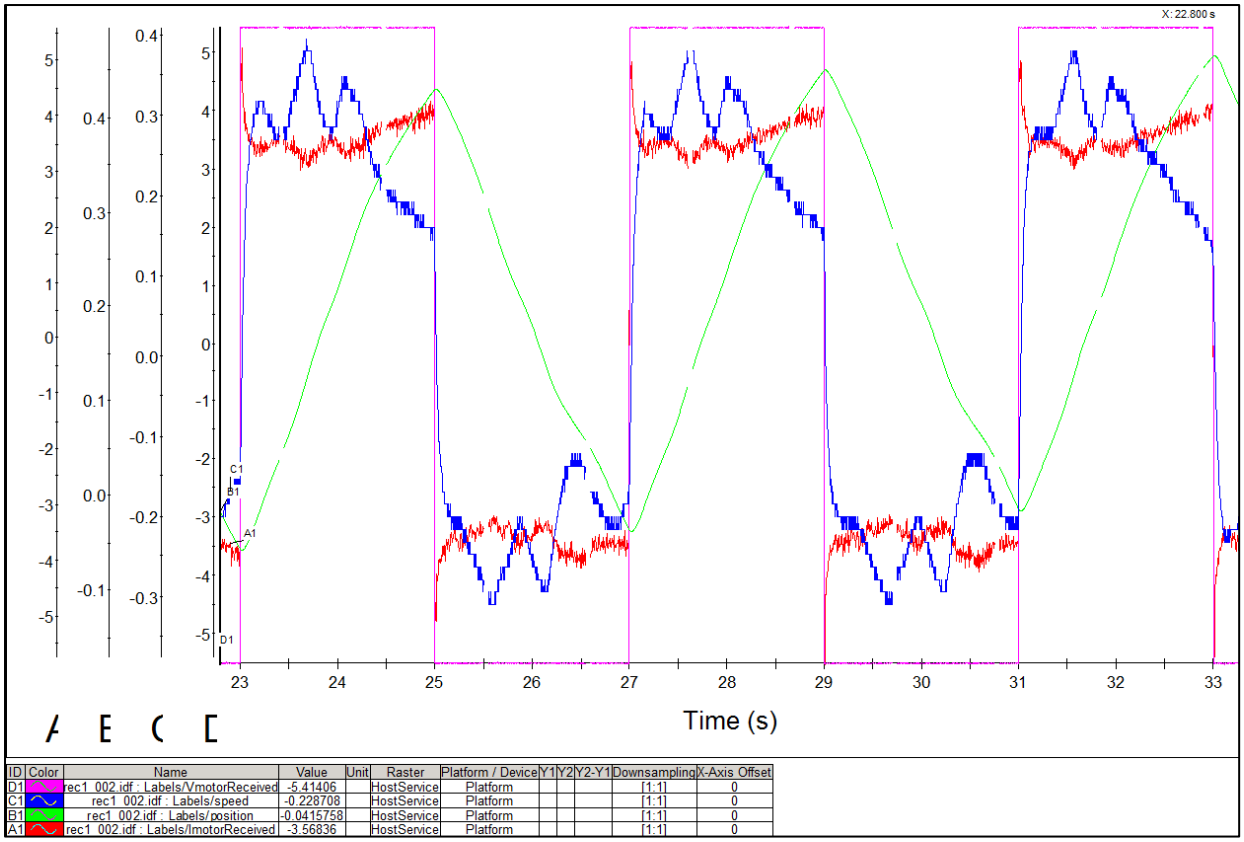

Figure 9: Current Drive Pulse Response

The same experiment was undertaken for the Voltage input (Figure 9), which resulted in a very similar outcome, and even a higher visualisation of the cart velocity readback throughout the rail length and thus the impact of the friction force on the movement of the cart. It is worth mentioning the fact that when Voltage is used to drive the cart, due to the resistance present in the motor, it will constantly drop, which will thus produce a change in current that can also be visualised in Figure 9.

Controller Design

4.1 Open-loop stability

In [27] it is stated that a system is asymptotically stable once its A matrix from the State-Space representation has all its eigenvalues in the left hand plane (Real part strictly negative). The eigenvalues of the system are given as:

Current

$$\begin{bmatrix} 0 \\ -5.0943 \\ -2.8305 \\ 4.2817 \end{bmatrix}$$

Voltage

$$\begin{bmatrix} 0 \\ 4.2136 \\ -7.4097 \\ -3.7944 \end{bmatrix}$$

Thus, for both cases the system is considered unstable. This phenomenon can also be visualised by analysing the open-loop response of the system through simulating a step signal fed to both the cart and the pendulum through the characteristic transfer function.

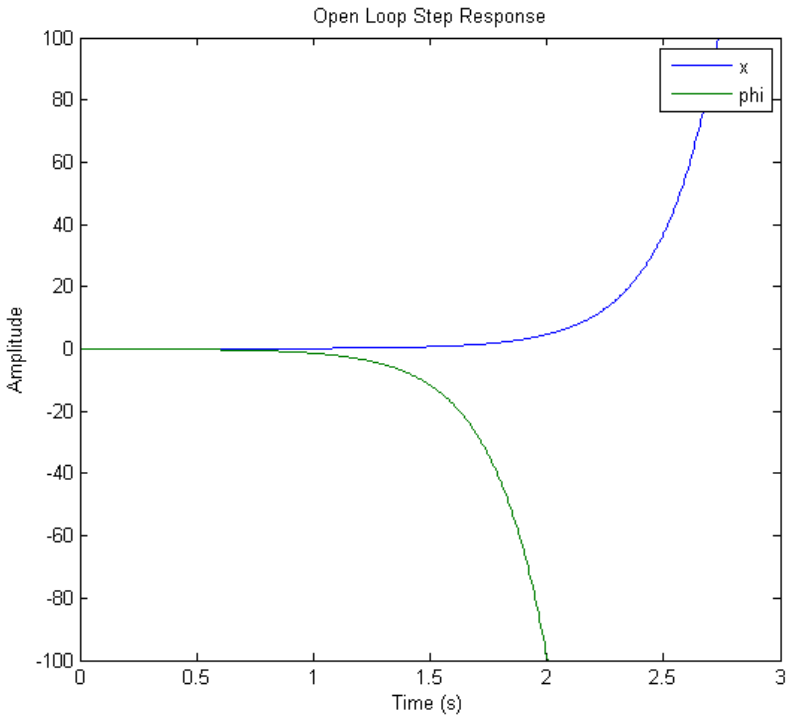

Figure 10: Open Loop Transfer Function Step Response

The outcome is represented in Figure 10 and the MATLAB code can be found in Appendix Id.

4.2 Linear Quadratic Regulator (LQR)

The chosen Controller to stabilize the system and obtain the needed outcome of recovering from disturbances is the LQR controller. It is particularly useful in helping balance the performance of the system with the magnitude of the inputs required to achieve that level of performance [37]. It is the one that behaves the best with non-linear system after linearization. One of the primary uses of feedback is to allow good performance in the presence of uncertainties, and hence requiring to have an exact model of the process is undesirable. An alternative to calibration is to make use of integral feedback, in which the controller uses an integrator to provide zero steady-state error [37]. The working principle and theory behind the LQR approach can be found in Appendix Va.

4.2.1 LQR MATLAB behaviour

Based on the LQR theory, the behaviour of the system was analysed after finding the K feedback gain using the discrete LQR MATLAB command.

Current (I)			**Voltage (V)**
No Dead Zone		**Dead Zone**	**No Dead Zone**
unfiltered	*filtered*	*filtered*	*filtered*
$Q = diag([1000, 1, 1000, 1])$	$Q = diag([400, 1, 700, 1])$	$Q = diag([55, 1, 580, 1])$	$Q = diag([400,1,700,1])$
$Q_R = 1$	$Q_R = 1$	$Q_R = 1$	$Q_R = 1$
$K = [-30.5919 \ -31.5916 \ -123.7538 \ -28.6351]$	$K = [-19.4070 \ -24.2971 \ -101.9407 \ -23.4733]$	$K = [-7.2231 \ -15.9656 \ -77.7324 \ -17.5079]$	$K = [-19.3516 \ -22.2838 \ -79.3598 \ -18.0547]$

Table 7: LQR fine-tuned gains (Highlighted = Best behaviour)

In Table 7, the parameters used for obtaining the feedback gains are presented. The LQR fine-tuning method is commonly used in such situations, and it is a time-consuming process [53]. Further on in the research, the gains will be used for simulations, further real-time experimentation, and will be recalled by the type of system accountability (unfiltered/filtered; (no) dead zone).

Every calculation of the K gain was carried out by applying the discrete time matrix A_d and B_d with a chosen sample time of $T_s = \frac{1}{200} s$ and a ZOH D/A Converter.

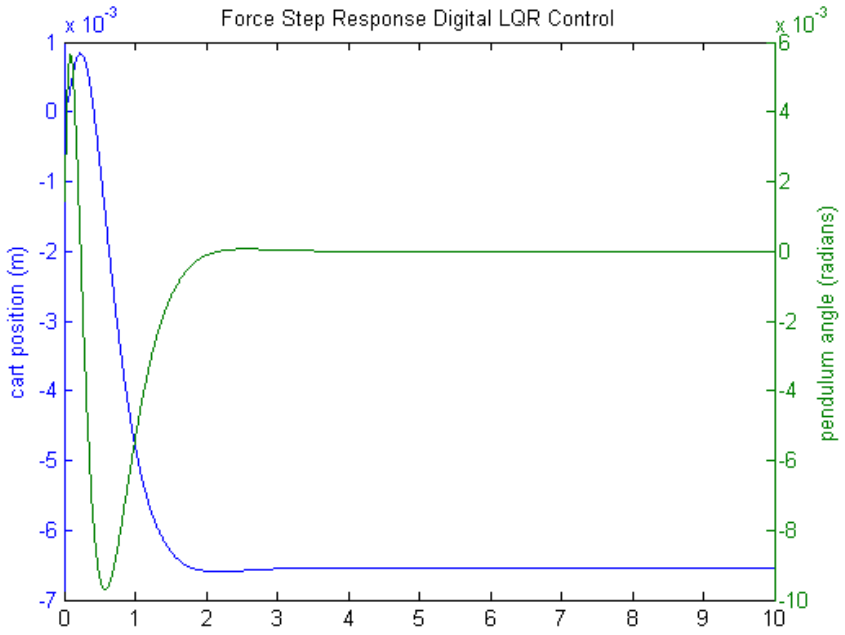

Figure 11a: Unfiltered Force MATLAB Closed-Loop Response

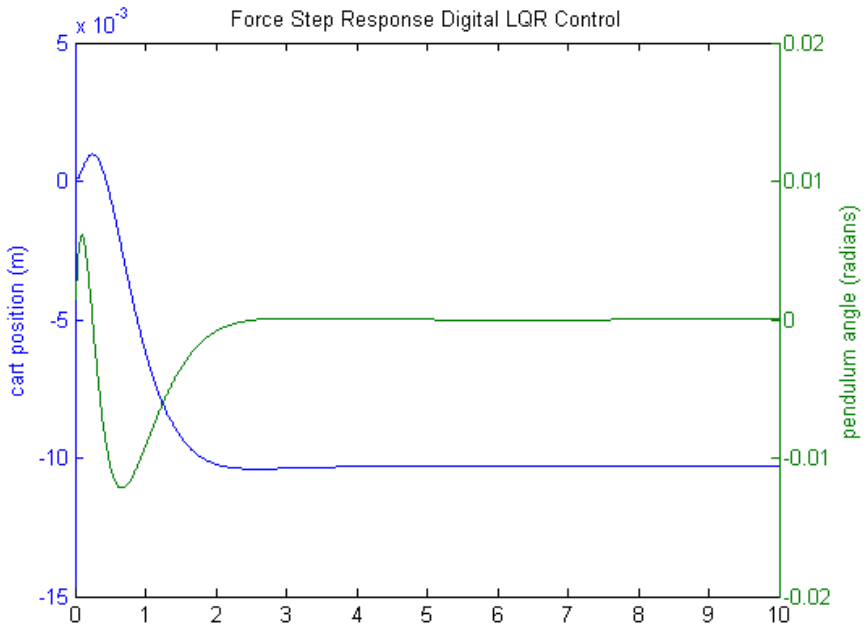

Figure 11b: Filtered Force MATLAB Closed-Loop Response

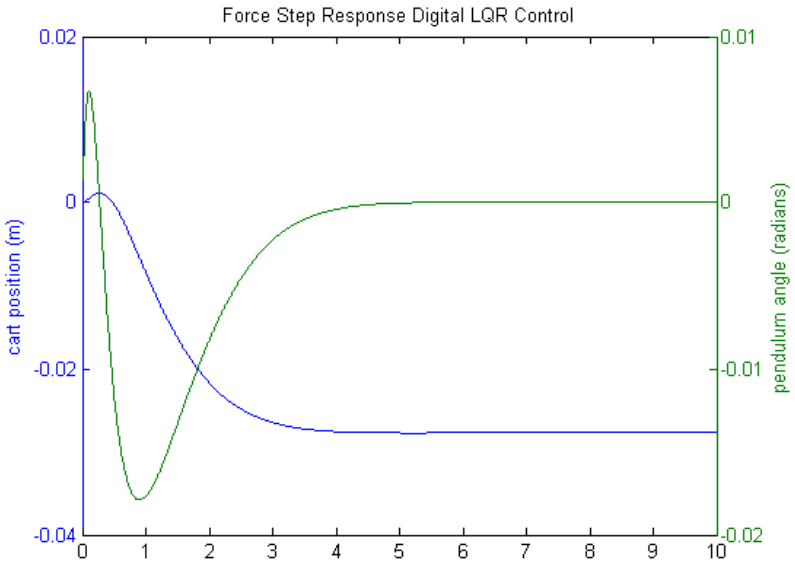

Figure 11c: Dead zone accounted filtered Force MATLAB Closed-Loop Response

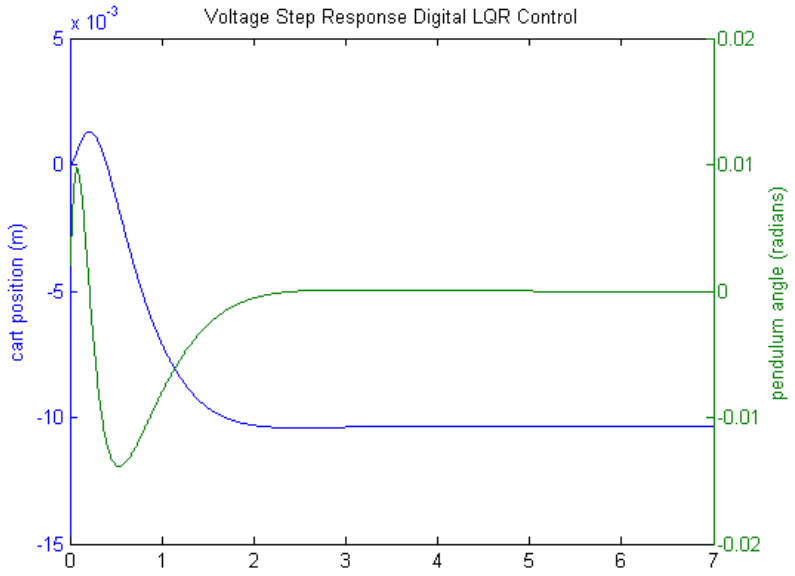

Figure 11d: Filtered Voltage MATLAB Closed-Loop Response

The Closed-Loop outcomes in a sequential order can be seen in Figures 11. If a step input is given to the system, the pendulum angle tends to 0, while the cart is displaced to the left. The angle of the pendulum is the most important part to analyse while the cart position is secondary as it should fit into the $[-0.5;\ 0.5]$ m range of displacement. The MATLAB code for the situations is given in Appendix I.

4.2.2 LQR Simulink Model & Simulation Behaviour

After identifying the needed gain by use of the LQR theory within the MATLAB file, a Simulink Model was built to show that indeed when the system is at a certain initial condition, it converges to a desired Steady State value. All the simulations are undertaken for the best outcome of the system (Highlighted one from Table 7) whose identification will be presented by the end of the report. It is worth noting that for all the LQR gains from Table 7 the outcome is very similar in terms of behaviour and they differ solely based on amplitudes.

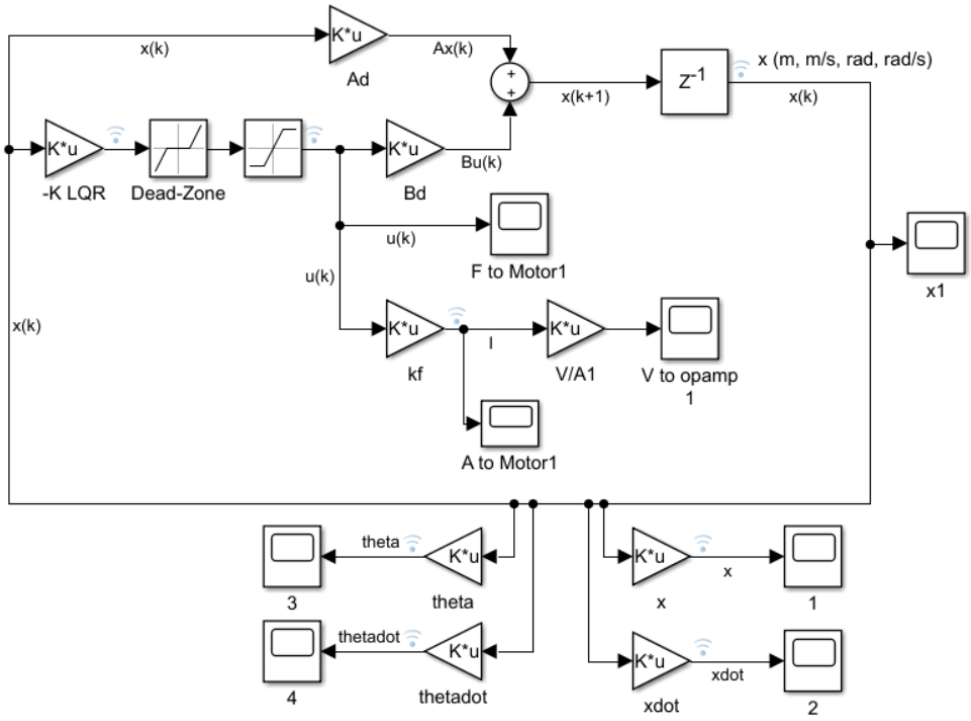

Figure 12a: Discrete Current LQR Simulink State Space Representation to Disturbance with Initial Conditions

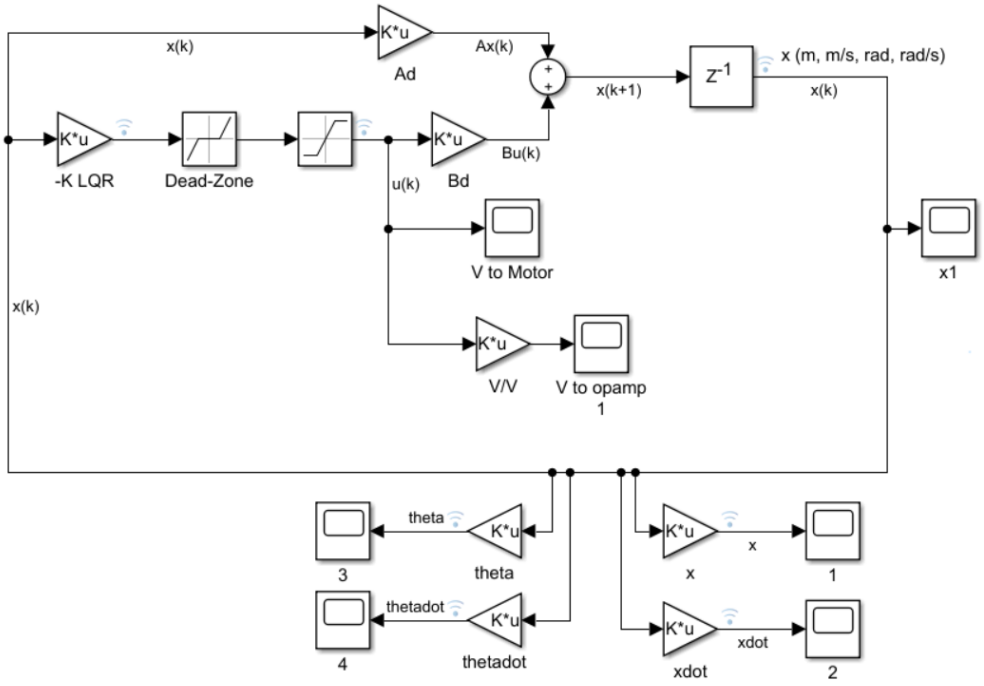

Figure 12b: Discrete Voltage LQR Simulink State Space Representation to Disturbance with Initial Conditions

Figures 12a & 12b show the blocks used to represent the State-Space representation by using the feedback gain K based on the feedback law: $u = -Kx$ together with an external disturbance in the form of a pendulum kick. It is worth mentioning that there is no reference point present since the system is stabilized around the equilibrium point:

$$\begin{bmatrix} x_e \\ \dot{x}_e \\ \theta_e \\ \dot{\theta}_e \end{bmatrix} = \begin{bmatrix} 0 \\ 0 \\ 0 \\ 0 \end{bmatrix} \tag{48}$$

To be able to see how the system behaves in the case a dead zone is present and a saturation limit exists, the Simulink blocks “Saturation” & “Dead Zone” were used as shown in Figure 12a. The region for the Dead Zone is taken as $[-2.51;\ 2.51]\ A$ for the current and for the voltage driven DC-Motor from Figure 12b, the region is $[-0.87;\ 0.87]\ V$. Furthermore, due to the fact that the op-amp drives the motor, its saturation should be accounted for; which will be also implemented in the experimental setup.

The initial conditions are arbitrarily given as:

$$\begin{bmatrix} x(0) \\ \dot{x}(0) \\ \theta(0) \\ \dot{\theta}(0) \end{bmatrix} = \begin{bmatrix} 0 \\ 0 \\ 0.2 \\ 0 \end{bmatrix} \tag{49}$$

With such Initial Conditions, the response after running the simulation given in Current mode and in Voltage mode is can be visualized in Figure 13a and Figure 13b respectively.

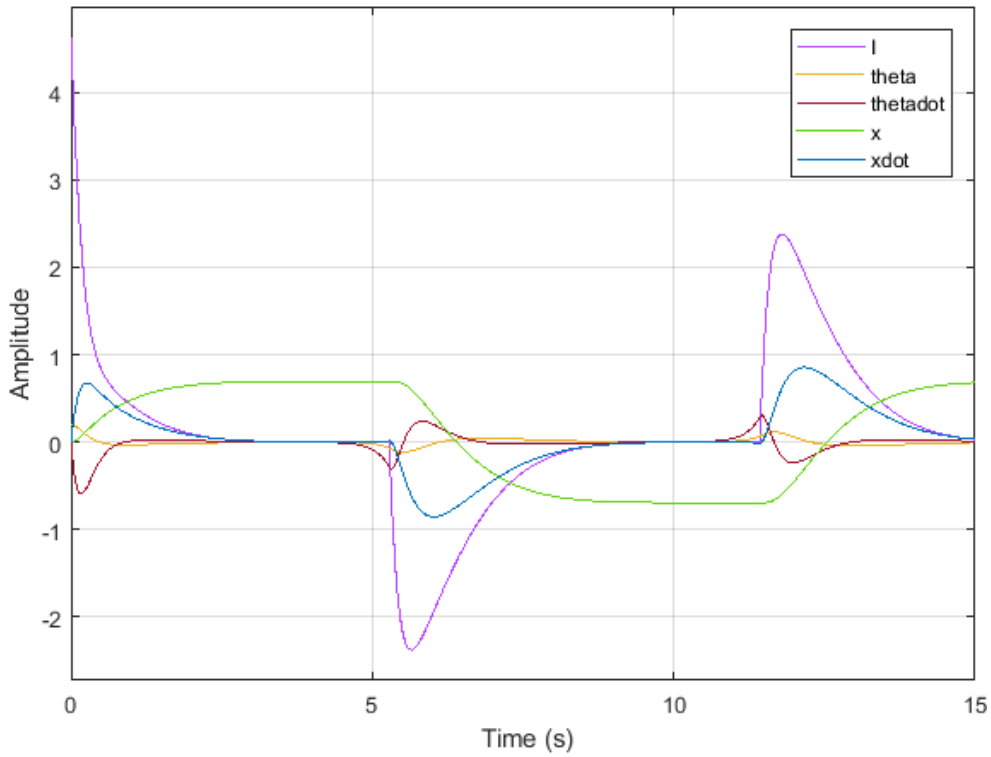

Figure 13a: Discrete Current Simulink Response (Dead Zone presence and Saturation)

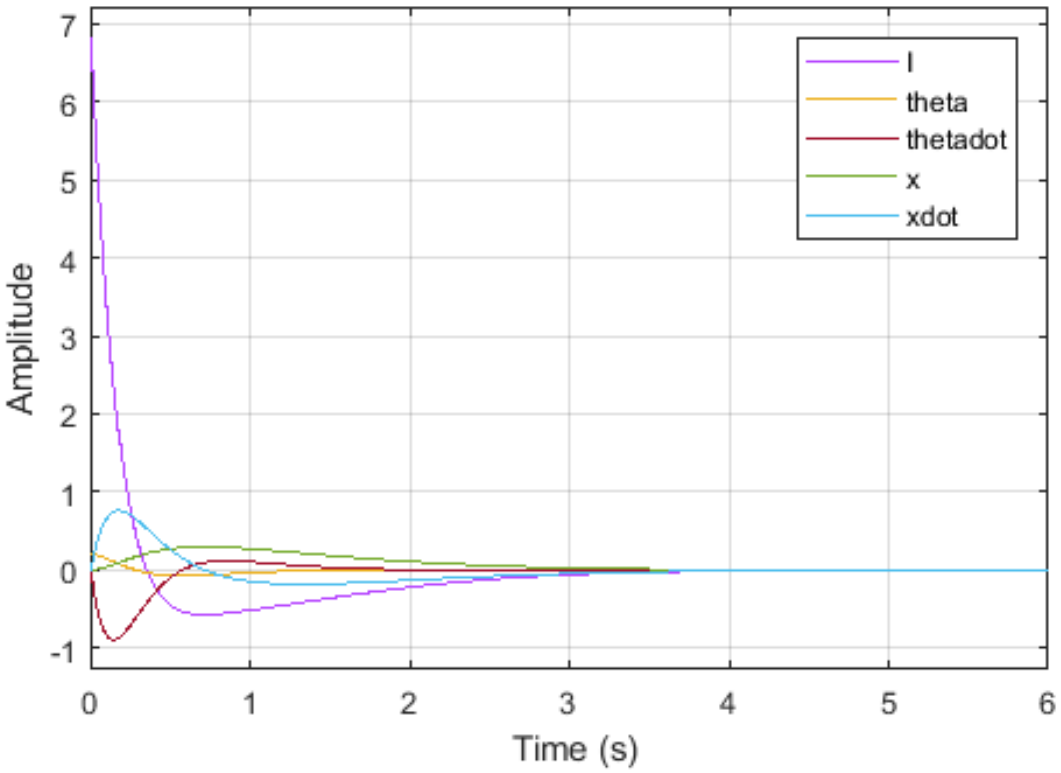

Figure 13b: Discrete Current Simulink Response (no Dead Zone)

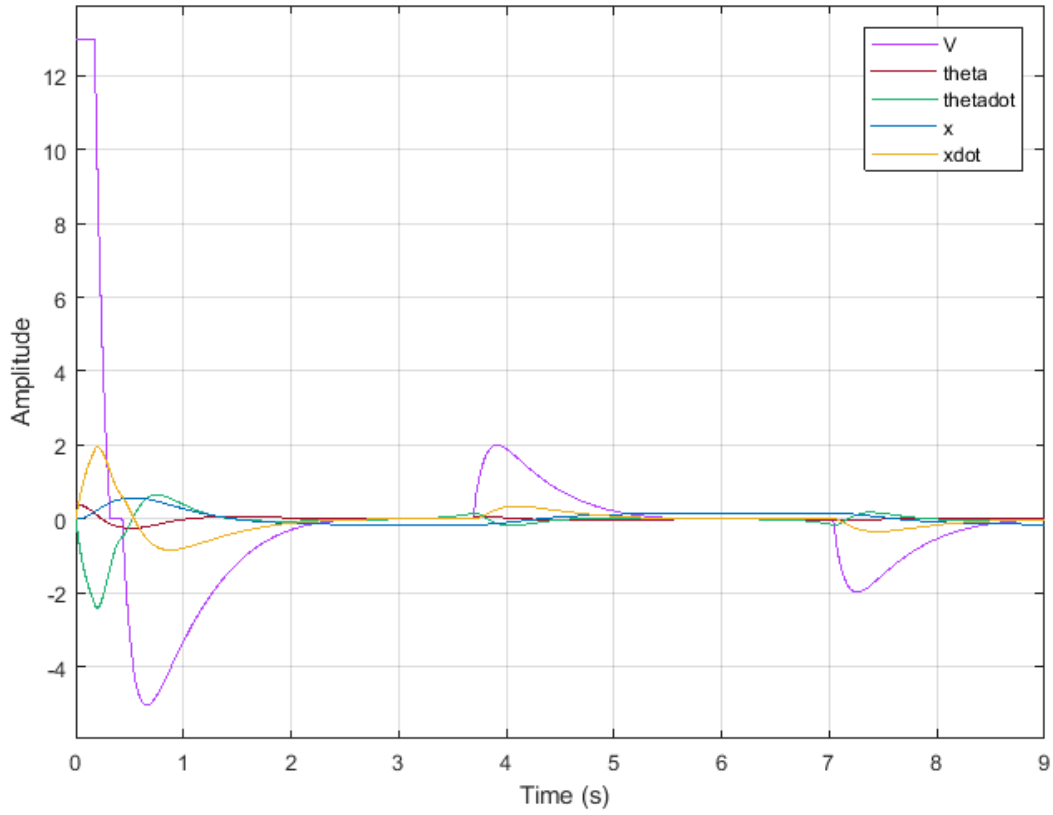

Figure 13c: Discrete Voltage Simulink Response (Dead Zone presence and Saturation)

As observed, after the disturbance is applied, both the Current and Voltage driven systems where the dead zone region is not accounted for do not reach a stop and the system continues to oscillate. This is the expected behaviour due to the presence of high static friction.

4.2.3 Critical Recovery

Based on the initial states set for the Simulink model, the moment at which the system instability will be reached can be found. As the angle of the pendulum represents the error between the reference value and the actual one, a trial and error approach was undertaken to find the maximum error for the angle by changing the initial condition for the angle while keeping the other state's initial condition at 0.

Thus, a maximum error threshold (based on the cart's maximum displacement threshold) was identified experimentally as $0.33\ rad = 18.9°$ for the Current driven case & $0.37\ rad = 21.2°$ for the Voltage driven one.

Experimental Overview

5.1 Setup (Workflow)

In order to proceed to testing the chosen controller on the system considered, the following steps have to be followed:

1. Run the MATLAB LQR Code
2. Choose the sampling time in Simulink Parameter Configuration as fixed-step with a sampling time T_s
3. Build the Simulink Model containing the dSPACE blocks
4. Visualize the variables of interest in the dSPACE Software and record the experiment
5. Start measuring the values
6. Bring the Pendulum to its vertical position
7. Tuning of the angle offset
8. Switch the op-amp to the correct DC-Motor supply
9. Turn on the op-amp
10. Analyse the behaviour of the system
11. Turn off the op-amp
12. Interpret the recorded values

5.2 System Behaviour Analysis

Firstly, the Current supplied DC-Motor situation was analysed.

Current (I)

In order to obtain the 4th state, which is the angular velocity of the pendulum $\dot{\theta}$, a discrete time derivative block was added to the pendulum angle sensor measurement. The Simulink Control scheme used for the real-life experimental implementation is given in Figure 15.

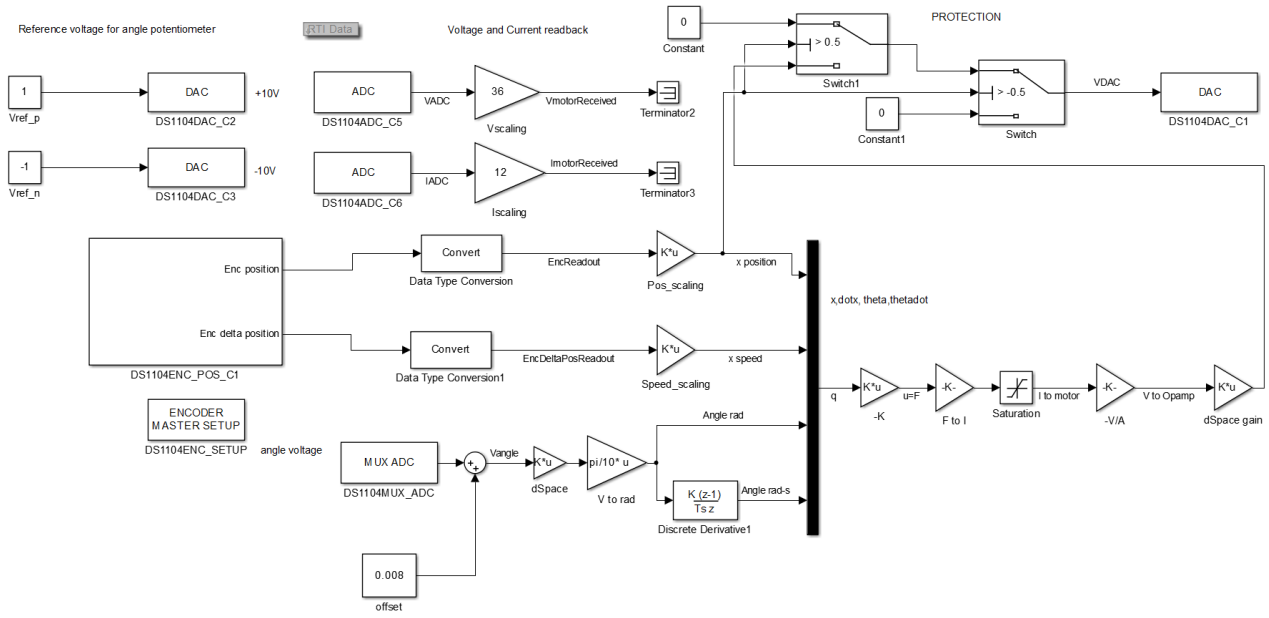

Figure 15: Simulink Current Input Connections

After following all the workflow steps, the results were recorded as follows:

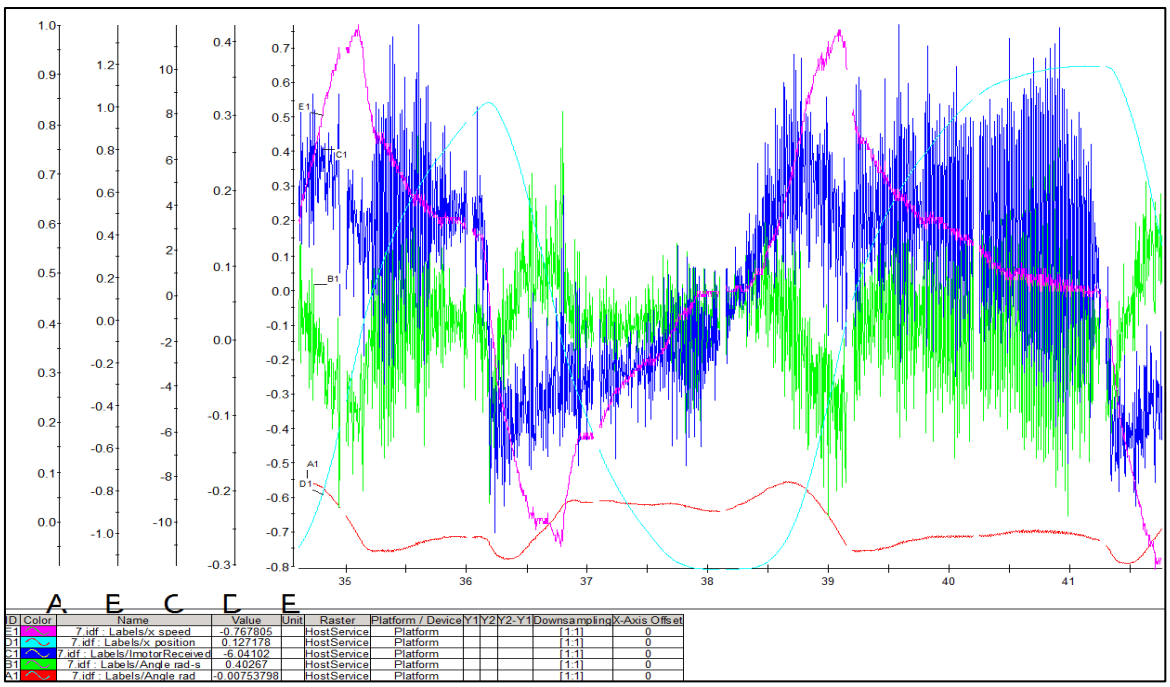

Figure 16: Experimental results for Current Input LQR

As can be seen in Figure 16, the measurement for the pendulum's angular velocity is a noisy one which in turn perturbates the system by creating noise in the input signal to the motor. Furthermore, the experiment produced undesirable oscillations of the system which does not lead to a stable situation and a solution to eliminate them has to be found.

A signal filtering method is one solution to the aforementioned problem. Another possibility is the design of an observer. Unfortunately, the observer design did not deliver the expected results and was thus, not chosen as the state estimator method for this setup. The design of a derivative filter was the chosen alternative solution which indeed provided the desired outcome [54]. Moreover, The discrete time derivative filter has 3 main variables which affect the performance of the filter: the derivative gain K, the time constant T (higher – less filtering, lower – more filtering), and the sample time which is chosen from the beginning at the MATLAB code generation stage. The value of the gain is a constant number chosen as 1, due to the fact that within this frame, by changing it (experimental analysis), the filter behaves worse. Currently, the derivative signal contains a great amount of noise which requires the filter to filter the signal more, thus implying a lower value for T. As a result, the value that gave the best results experimentally, was $T = 0.01$.

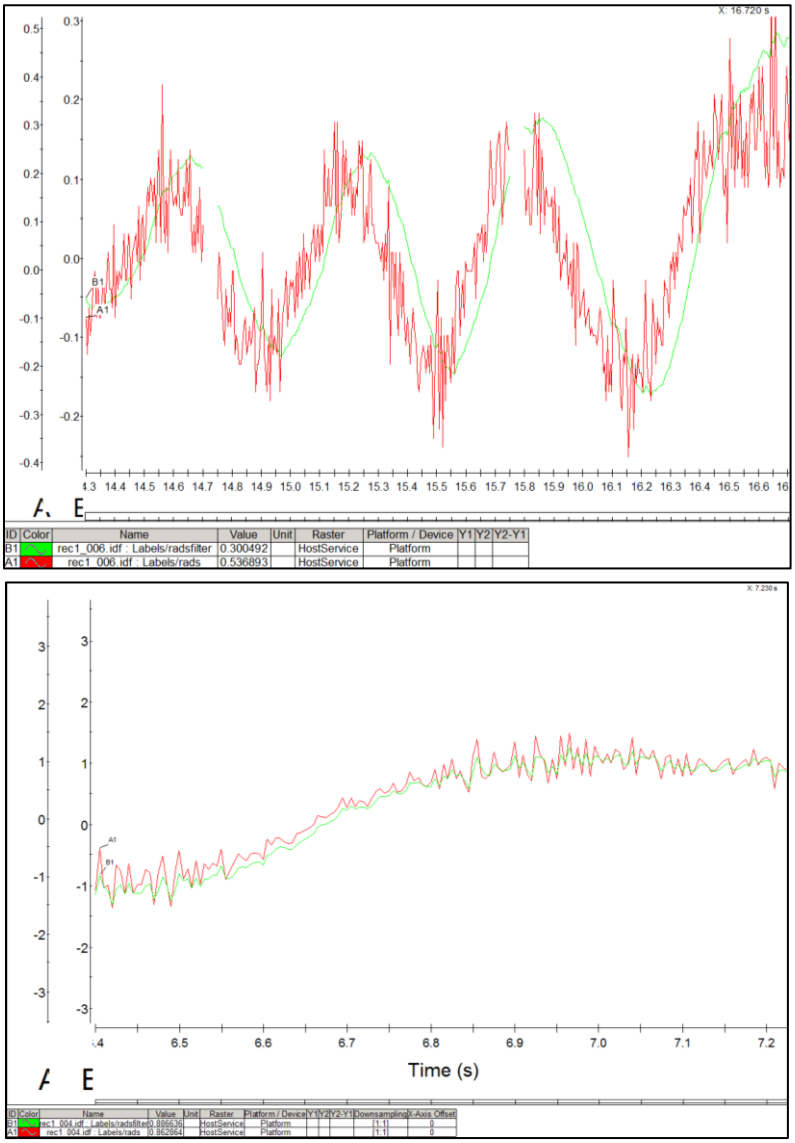

Figure 17: Filtered vs Original Derivative of $\dot{\theta}$

The outcome of the filtering procedure can be seen in Figure 17.

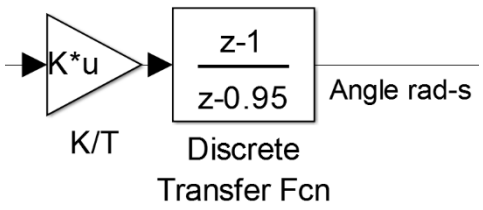

Figure 18: Discrete Filtered Derivative

Thus, the discrete derivative block from Figure 15, is replaced with the one in Figure 18.

The gains of the Q matrix had to be adjusted since the system was not stable anymore after filtering.

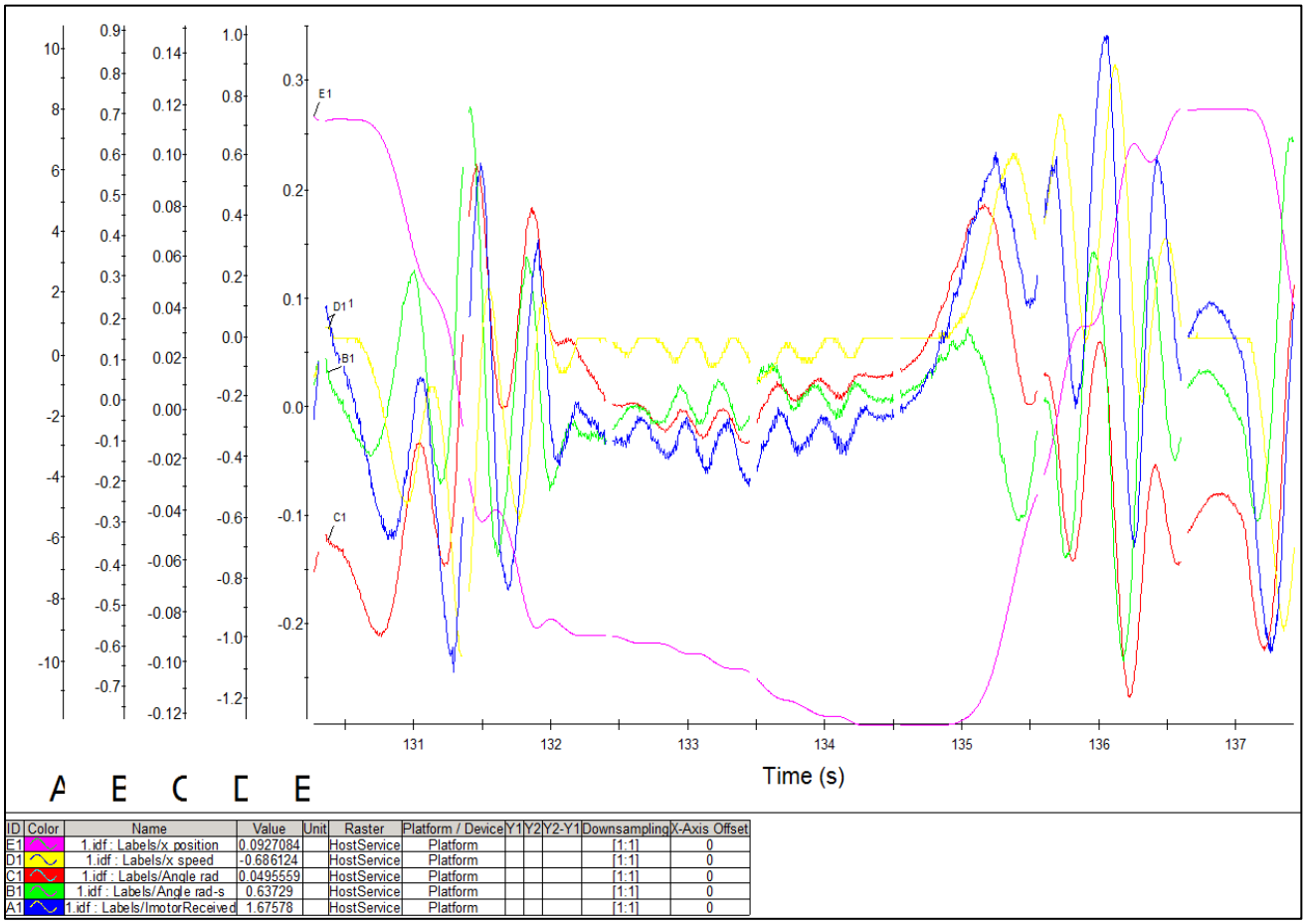

ID	Color	Name	Value	Unit	Raster	Platform / Device	Y1	Y2	Y2-Y1	Downsampling	X-Axis Offset
E1		1.idf : Labels/x position	0.0927084		HostService	Platform				[1:1]	0
D1		1.idf : Labels/x speed	-0.686124		HostService	Platform				[1:1]	0
C1		1.idf : Labels/Angle rad	0.0495559		HostService	Platform				[1:1]	0
B1		1.idf : Labels/Angle rad-s	0.63729		HostService	Platform				[1:1]	0
A1		1.idf : Labels/ImotorReceived	1.67578		HostService	Platform				[1:1]	0

Figure 19: Experimental results for filtered Current Input LQR (no dead zone account)

As can be seen in Figure 19, after implementation, the experimental results change and the amount of noise in the system is considerably reduced. Furthermore, the behaviour of the system becomes more stable, which is confirmed by the fact that the cart velocity is small for a short moment of time until the pendulum starts falling again due to its low friction pivot.

As the goal of reaching absolute stability was not yet reached and the system still oscillates while travelling on the rail, the integration of the dead zone region was considered. The offset point for the Force to Current conversion was added by replacing the $I = 0.4392F$ gain block from Simulink with a MATLAB function given in Appendix 1e. Due to the fact that the pendulum needs a dead zone region for the angle which it would consider as the stability point, the condition in the MATLAB code from Appendix 1e states that there is no control signal in the region where the force is between $\pm 1\ N, as\ it\ corresponds\ to \sim \pm\ 0.5\ A$. A further adjustment of the LQR gains was needed which provided a much better response of the system.

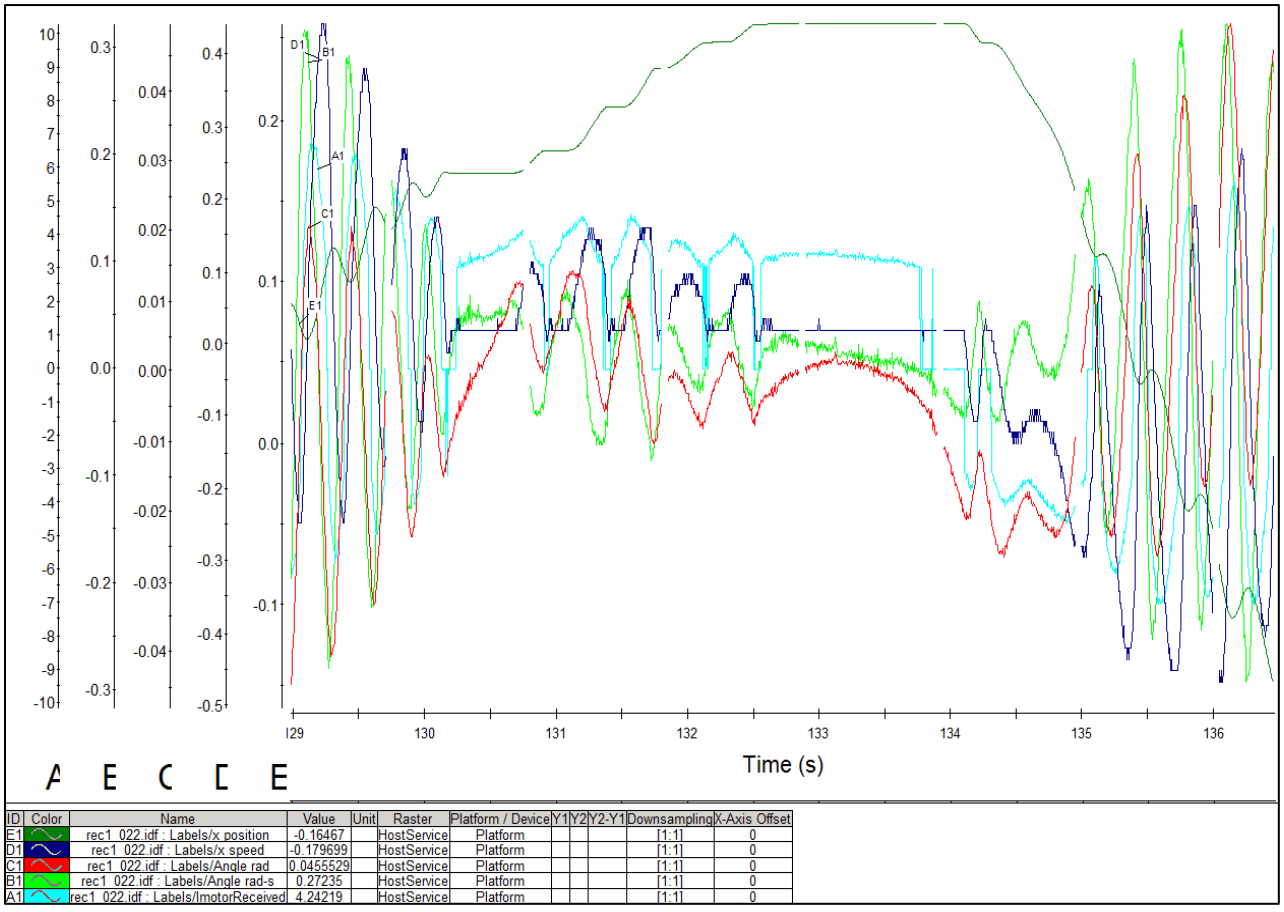

Figure 20: Experimental results for the Dead zone accounted and filtered Current Input LQR [56]

The gains that gave the best outcome, triggered the cart to stay within a close range of the reference point with little amplitude oscillations and the pendulum to maintain its upright position while sometimes even achieving absolute stability for a short period of time (132.5 *sec* – 134 *sec Figure* 20). The actual real-time behaviour can also be seen by accessing the video source [56]. Furthermore, after applying disturbance, the cart as well as the pendulum responded very well by returning back to their reference points.

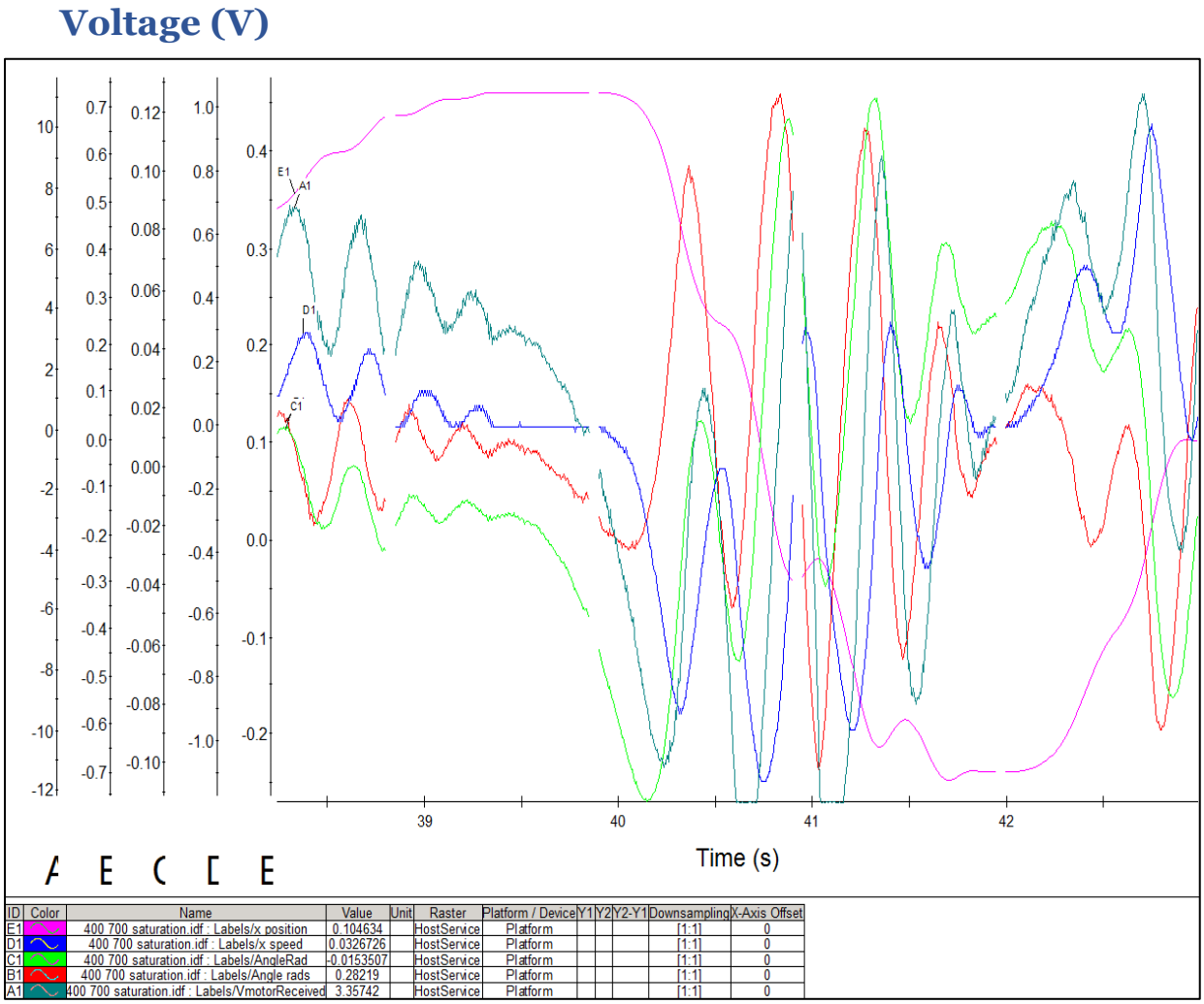

Figure 21: Experimental results for filtered Voltage Input LQR (no dead zone account)

Due to the fact that the voltage driven system contains a greater number of constants and variables that describe the DC Motor's behaviour, the system was analysed till the point where it could keep the pendulum in an upright oscillatory position. The complex modelling, the fact that due to the DC Motor's resistance a voltage drop as well as the constraint of time for perfecting the experiment, placed this input as a second choice.

Conclusion

6.1 Goal fulfilment

The work done during this research on the stabilization problem was an indispensable opportunity to test the knowledge of the classical control systems theory. Thus, the behaviour and success of the LQR control law on the Single-Input/Multiple-Output (SIMO) system confirms the feasibility of the software and hardware that was employed in this experimental setup. As expected, due to a highly non-linear system at hand, the behaviour after the real-time experiment was used differs from the simulated one. In reality, the system cannot be fully defined, and the modelling of each component is non-linear in itself and by not being able to exactly characterize the components, the system behaviour cannot be predicted.

Based on the outcome of the experiments, the best behaving control signal is the one where current is used to drive the DC-Motor. The noise filtered system in which the dead zone is accounted for, returned the best results and kept the pendulum upright with relatively little amplitude oscillations. Furthermore, a fine-tuning trial and error approach of finding the LQR gains was applied and as can be seen in Figure 7, the chosen best performing situation is the 3rd one.

The pendulum is maintained it its upright position and comes to a full stop for a period of time, while the cart oscillates within the $\pm 0.25\ m$ region which shows that the stabilization goal was achieved. Similarly, the low friction bearing ($B = 0$) also influences the stabilization as the pendulum will rarely be able to hold the exact upright position as it tends to continue moving. The choice of Current over the Voltage driven DC-Motor can be explained by the fact that once the Voltage drive is used, a voltage drop is experienced due to the motor's characteristics.

While testing the setup, the behaviour of the system could the constantly improved by perfecting the separate components as well as by further tuning. Thus, the system can indeed be upgraded so as to behave in the best desired way possible, by achieving absolute stability without oscillations.

The theoretical analysis that was carried out confirms the fact that the system behaviour is sensitive to mathematical model changes of the cat-pendulum system as well as to the DC motor modelling. These are therefore important for stability and a good performance of the controller.

6.2 *Future Work*

For future work, the investigation of the non-linear control strategy implementation has to be considered due to the non-linearities that are currently present in the system. To further improve the behaviour and performance of the cart and pendulum, the friction factor has to be reduced or at least normalized throughout the rail length. Another possibility of improving the existing output is further fine-tuning of the gains or even the implementation of the Proportional Integral Derivative (PID) controller as the task of stabilization can be attained by tuning the PID gains which does not require a precise modelling of the system.

Bibliography

[1] Discrete Technology & Production Automation (DTPA) Available at: Https://Www.Rug.Nl/Research/Discrete-Technology-Production-Automation/

[2] Chakraborty, S. (2014). *An Experimental study for Stabilization of Inverted Pendulum*. [online] Available at: http://ethesis.nitrkl.ac.in/5561/1/E-THESIS_32.pdf

[3] Control Systems Lab (Sc4070). *Inverted Pendulum Experiment*. Available At: Http://Www.Dcsc.Tudelft.Nl/~Sc4070/Transp/Labinvpend.Pdf

[4] Gustavsson, M., & Frimodig, V. (2015). *Virtual Prototyping and Physical Validation of an Inverted Pendulum: 'Sea-Calf Bot' (Dissertation)*. Available at: http://urn.kb.se/resolve?urn=urn:nbn:se:hh:diva-27946

[5] Jason, K. (2017). *Difference Between an Incremental Encoder's PPR, CPR, and LPR*. Available at: https:// cui.com/blog/what-is-encoder-ppr-cpr-and-lpr

[6] Hasan, M., Saha, C., Rahman, M., Sarker, M. and Aditya, S. (2012). *Balancing of an Inverted Pendulum Using PD Controller*. Dhaka University Journal of Science, 60(1), pp. 115-120. doi: 10.3329/dujs.v60i1.10348.

[7] Sultan, K. (2003). *Inverted Pendulum Analysis, Design and Implementation*. Available at: http://engr.usask.ca/classes/EE/480/Inverted%20Pendulum.pdf

[8] Magaña, M.E., & Holzapfel, F. (1998). *Fuzzy-logic control of an inverted pendulum with vision feedback*. IEEE Transactions on Education, *41*, 165-170.

[9] Toliyat, H. A., Abolhassani, M., Niazi, P., Hao, L. (2018). 39 - DSP-Based Control of Variable Speed Drives, *Power Electronics Handbook (Fourth Edition)*, Pages 1303-1323, ISBN 9780128114070. Available at: https://doi.org/10.1016/B978-0-12-811407-0.00043-X.

[10] Adewusi, S. (2016). *Modeling and Parameter Identification of a DC Motor Using Constraint Optimization Technique*. IOSR Journal of Mechanical and Civil Engineering (IOSR-JMCE). 13. 46-56. 10.9790/1684-1306024656.

[11] Kelechukwu, S. A. (2019*). Standup and stabilization of the inverted pendulum*.

[12] *Reading The Motor Constants From Typical Performance Characteristics* - Precision Microdrives. Available at:

https://precisionmicrodrives.com/content/reading-the-motor-constants-from-typical-performance-characteristics/

[13] *Understanding DC Motors*. Available at: http://me.umn.edu/courses/me2011/arduino/technotes/dcmotors/motor-tutorial/

[14] *Test Equipment Solutions Datasheet* - KEPCO-BOP36-12M-Datasheet. Available at: http://www.testequipmenthq.com/datasheets/KEPCO-BOP36-12M-Datasheet.pdf

[15] Messikh, L & Guechi, Elhadi & Benloucif, M.L. (2017). *Critically Damped Stabilization of Inverted-Pendulum Systems Using Continuous-Time Cascade Linear Model Predictive Control*. Journal of the Franklin Institute. 354.10.1016/j.jfranklin.2017.08.039.

[16] Campbell, Sue & Crawford, Stephanie & Morris, Kirsten. (2008). *Friction and the Inverted Pendulum Stabilization Problem. Journal of Dynamic Systems Measurement and Control-transactions of The Asme* - J DYN SYST MEAS CONTR. 130. 10.1115/1.2957631.

[17] *Potentiometer Transducers or Sensors*. Available at: https://brighthubengineering.com/hvac/47389-what-is-potentiometer-potentiometer-used-as-the-transducer-or-sensor/

[18] Li, Z., Chenguang, Y., Liping, F. (2014). *Advanced Control of Wheeled Inverted Pendulum Systems*. Doi:10.1007/978-1-4471-2963-9.

[19] Varghese, E.S., Anju, K.V., Bagyaveereswaran, V. (2017). *Optimal Control of Inverted Pendulum System Using PID Controller*, LQR And MPC. Doi:10.1088/1757-899X/263/5/052007

[20] Jose, A., Clint, A., Shinu, M. M., Keerthi, C. (2015). *Performance Study of PID Controller and LQR Technique for Inverted Pendulum*. World Journal of Engineering and Technology. 03. 76-81. 10.4236/wjet.2015.32008.

[21] Hevner, Alan R. (2007). *A Three Cycle View of Design Science Research*, Scandinavian Journal of Information Systems: Vol. 19: Iss. 2, Article 4. Available at: http://aisel.aisnet.org/sjis/vol19/iss2/4

[22] Nygren, F. S. A. (2015). *Controller Analysis With Inverted Pendulum*. Available at: http://diva-portal.se/smash/get/diva2:916306/FULLTEXT01.pdf

[23] *Potentiometer* – Wikipedia. Available at: https://en.wikipedia.org/wiki/Potentiometer

[24] HEDL-550x/554x - *Avago Technologies Encoder Data Sheet*. Available at: https://maxonmotor.com/medias/sys_master/root/8814444773406/AV02-0993EN.pdf

[25] Kostik, B. (2011). *Potentiometers: A Proven Position Sensing Solution that Every Engineer Needs to Consider in Modern Designs*. Available at: https://www.sensorsmag.com/embedded/potentiometers-a-proven-position-sensing-solution-every-engineer-needs-to-consider-modern

[26] Brock, S. (2002). *Identification of the parameters in inverted pendulum model [DC motor control]*. 7th International Advanced Motion Control, 2002.

[27] Åström, K. J., Murray, R. M. (2016). *Feedback Systems: An Introduction for Scientists and Engineers*. Princeton University Press, Princeton and Oxford.

[28] Jadlovska, S. & A. (2009). *A Simulink Library for Inverted Pendula Modeling and Simulation*.

[29] Teixeira, T. H., Siqueira, V., Munaro, C. (2011). *Comparison of methods for estimation and compensation of friction applied to an inverted pendulum*. IEEE International Conference on Control and Automation, ICCA. 818-823. 10.1109/ICCA.2011.6138033.

[30] Olsson, H., Åström, K. J., Canudas de Wit, C., Gafvert, M., Lischinsky, P. (1998). *Friction Models and Friction Compensation*. *European Journal of Control*. 4. 10.1016/S0947-3580(98)70113-X.

[31] Collins, D. (2015). *Encoder Resolution*. Available at: https://linearmotiontips.com/how-encoder-resolution-is-determined/

[32] *Moment of inertia* – Wikipedia. Available at: https://en.wikipedia.org/wiki/Moment_of_inertia

[33] Deriso, J. (2015). Potentiometer Basics. Available at: https://os.mbed.com/components/Potentiometer/

[34] Seto, D., Sha, R. L. (1999). *A Case Study on Analytical Analysis of the Inverted Pendulum Real-Time Control System* (CMU/SEI-99-TR-023). Retrieved May 19, 2019, from the Software Engineering Institute, Carnegie Mellon University website: http://resources.sei.cmu.edu/library/asset-view.cfm?AssetID=13511

[35] Fajar, M (2014). *Conceptual Design and Simulation of An Inverted Pendulum Wheelchair*. Masters thesis, Liverpool John Moores University.

[36] Chen, Y. P. (2015). *Dynamic System Simulation and Implementationon (Modelling of a DC Motor)*. Available at: http://ocw.nctu.edu.tw/course/dssi032/DSSI_2.pdf

[37] Åström, K. J., Murray, R. M. (2008). *Feedback Systems: An Introduction for Scientists and Engineers*. Princeton University Press, Princeton and Oxford.

[38] Redlich, M., Tenne, R. (2013). *Chapter 13 - Nanoparticle Coating of Orthodontic Appliances for Friction* Reduction. Available at: https://doi.org/10.1016/B978-1-4557-3127-5.00013-1.

[39] Geffen, V. (2009). *A study of friction models and friction compensation*. Available at: http://mate.tue.nl/mate/pdfs/11194.pdf

[40] Miller, G. (1997). *Nonlinear model-based friction compensation in control systems: Theory and Experiment*. Available at: https://collectionscanada.gc.ca/obj/s4/f2/dsk2/ftp04/mq20673.pdf

[41] Orozco, Q. R. (2009). *Pendulum-Cart System -User's Manual Pendulum-Cart System User's Manual*. Available at: https://academia.edu/15159215/Pendulum-Cart_System_-Users_Manual_Pendulum-Cart_System_Users_Manual

[42] Isotec - Eco Module. Available at: https://www.isotec.at/en/1459372/Products-Modules-Eco-modules

[43] Landry, M., Campbell, S., Morris, K., Aguilar, O. C. (2005). Dynamics of an Inverted Pendulum with Delayed Feedback Control. Siam Journal on Applied Dynamical Systems - SIADS. 4. 10.1137/030600461.

[44] Sidhu, K. (2012). *Understanding Linear Position Sensing Technologies*. Available at: https://sensorsmag.com/components/understanding-linear-position-sensing-technologies

[45] Siuka, A., Schoberl, M. (2009) *Applications of energy based control methods for the inverted pendulum on a cart*. Available at: https://doi.org/10.1016/j.robot.2009.07.016.

[46] Serway Physics for Scientists and Engineers 4th edition (p. 126.)

[47] Fenske, G., Erck, R., Ajayi, L., Erdemir, A., Eryilmaz, O. Parasitic (2006). *Energy Loss Mechanisms Impact on Vehicle System Efficiency*, Argonne National Laboratory. Available at: http://diracdelta.co.uk/science/source/f/r/friction/source.html#.XO__aLdR1PY

[48] Beardmore, R. (2013). *Surface Friction*. Available at: http://roymech.co.uk/Useful_Tables/Tribology/class_Friction.html

[49] Julius, O. S. (2010). *Physical Audio Signal Processing*. Available at: https://ccrma.stanford.edu/~jos/pasp/Newton_s_Laws_Motion.html

[50] Armstrong-H´elouvry, B., (1991). *Control of Machines with Friction*. Kluwer, Boston

[51] Jørgensen, J. H., Nielsen, Ø. J. (2018). Non-linear Control and Machine Learning on an Inverted Pendulum on a Cart.

[52] Gohari, P. (2006). Lecture 6: Discrete Equivalents. Available at: http://web.cecs.pdx.edu/~tymerski/ece452/6.pdf

[53] Verlie, J. (2017). Control of an Inverted Pendulum with Deep Reinforcement Learning.

[54] Filtered Derivative (Discrete or Continuous). Available at: https://nl.mathworks.com/help/physmod/sps/ref/filteredderivativediscreteorcontinuous.html

[55] Holzapfel, F. G. (1994). Fuzzy Logic Control of an Inverted Pendulum with Vision Feedback.

[56] Inverted Pendulum Demonstrator Video. Available at: https://youtu.be/8bqt_pt3v0A

Appendices

Appendix I – M-files

Appendix Ia - Current

```
%% System Parameters
clc
clear all
M = 1.3032;                 %kg
m = 0.277;                  %kg
b = 5.13;                   %N*s/m
l = 0.434;                  % m %center of gravity length
Ip = (1/3)*m*(l^2);         % kg*m^2 % I = 0.0174
g = 9.80655;                %m/s^2 or N/kg
kf = 0.439;                 %A/N

p=1-(((m*l)^2)/((M+m)*(Ip+m*l^2)))

% State Space Representation
A = [0 1 0 0; 0 -b/((M+m)*p) -(m*l)^2*g/(((M+m)*(Ip+m*l^2))*p) 0; 0 0 0 1;
0 m*l*b/((M+m)*(Ip+m*l^2)*p) m*l*g/((Ip+m*l^2)*p) 0]
B = [0; 1/((M+m)*p); 0; -m*l/((Ip+m*l^2)*(M+m)*p)]
C = [1 0 0 0; 0 1 0 0; 0 0 1 0];
D = [0; 0; 0];

% Discrete-time State-Space Model
states = {'x' 'x_dot' 'phi' 'phi_dot'};
inputs = {'F'};
outputs = {'x'; 'x_dot'; 'phi'};

sys_ss=
ss(A,B,C,D,'statename',states,'inputname',inputs,'outputname',outputs);

Ts = 1/200;
sys_d = c2d(sys_ss,Ts,'zoh');

% Controllability and observability
co = ctrb(sys_d);
ob = obsv(sys_d);

controllability = rank(co); % 4
observability = rank(ob); % 4
%This proves that our discrete system is both completely state controllable
%and completely state observable.

% LQR
Ad = sys_d.a;
Bd = sys_d.b;
Cd = sys_d.c
Dd = sys_d.d;
```

```
Q=diag([55,1,580,1]); % 1000 1 100 1
R = 1;
[K] = dlqr(Ad,Bd,Q,R)

Ac = [(Ad-Bd*K)];
Bc = [Bd];
Cc = [Cd];
Dc = [Dd];

states = {'x' 'x_dot' 'phi' 'phi_dot'};
inputs = {'F'};
outputs = {'x'; 'x_dot'; 'phi'};

sys_cl=
ss(Ac,Bc,Cc,Dc,Ts,'statename',states,'inputname',inputs,'outputname',output
s);

t = 0:0.005:10;
rc =0.2*ones(size(t));
[y,t,x]=lsim(sys_cl,rc,t);
[AX,H1,H2] = plotyy(t,y(:,1),t,y(:,2),'plot');
set(get(AX(1),'Ylabel'),'String','cart position (m)')
set(get(AX(2),'Ylabel'),'String','pendulum angle (radians)')
title('Force Step Response Digital LQR Control')
```

Appendix Ib – Voltage

```
%% System Parameters
clear all
clc
m = 0.277;              %kg
l = 0.434;              % m %centre of gravity length
M = 1.3032;             % kg
Ip= (1/3)*m*(l^2);      % kg*m^2
g = 9.80655;            %m/s^2 or N/kg
kg=1;                   %-
kt=0.0592;              %N*m/A
ke=0.0592;              %V*s/rad
R=1.1;                  %Ohm
r=0.026;                %m
Bm=0.0000764;           %N*m*s/rad
J=0.000035;             %kg*m^2
kf = 0.439;             %A/N
b = 5.13;               %N*s/m

p=1-(((m*l)^2)/((M+m)*(Ip+m*l^2)))
Z=1+J*kg/(r^2*(M+m)*p)

% State Space Representation
A = [0 1 0 0 ; 0 -(Bm*kg/r^2+kt*ke*kg^2/(r^2*R)+b)/((M+m)*p*Z) -
((m*l)^2*g)/((M+m)*(Ip+m*l^2)*Z)      0;      0      0      0      1;      0
m*l*((kg*Bm/r^2)+((kt*ke*kg^2)/(r^2*R))+b)/((Ip+m*l^2)*(M+m)*p*Z)
m*l*g/(Ip+m*l^2)+(m*l)^3*g/((M+m)*(Ip+m*l^2)^2*Z) 0]
B = [0; (kt*kg)/(r*R*(M+m)*p*Z); 0; -(m*l*kt*kg)/(r*R*(Ip+m*l^2)*(M+m)*p*Z)]
C = [1 0 0 0; 0 1 0 0; 0 0 1 0]
```

```
D = [0; 0; 0];

% Discrete-time State-Space Model

states = {'x' 'x_dot' 'phi' 'phi_dot'};
inputs = {'V'};
outputs = {'x'; 'x_dot'; 'phi'};

sys_ss                                                                    =
ss(A,B,C,D,'statename',states,'inputname',inputs,'outputname',outputs);

Ts = 0.005;

sys_d = c2d(sys_ss,Ts,'zoh');

% Controllability and observability

co = ctrb(sys_d);
ob = obsv(sys_d);

controllability = rank(co); % 4 Therefore, we have verified that our system
%is controllable and thus we should be able to design a controller that
%achieves the given requirements.
observability = rank(ob); % 4

%This proves that our discrete system is both completely state controllable
%and completely state observable.

% LQR
Ad = sys_d.a;
Bd = sys_d.b;
Cd = sys_d.c;
Dd = sys_d.d;

Q=diag([400,1,700,1]); %1000 1 200 1
R=1;
[K] = dlqr(Ad,Bd,Q,R)

Ac = [(Ad-Bd*K)];
Bc = [Bd];
Cc = [Cd];
Dc = [Dd];

polesa=eig(A)';
polesac=eig(Ac)';     % have to be in a circle of radius 1
polesak=eig(A-B*K)' ;   % all closed loop poles stable -1.9828 + 0.0000i  -
0.0101 - 0.0151i  -0.0101 + 0.0151i  -0.0171 + 0.0000i

states = {'x' 'phi' 'x_dot' 'phi_dot'};
inputs = {'V'};
outputs = {'x';'x_dot'; 'phi'};
```

```
sys_cl                                                                    =
ss(Ac,Bc,Cc,Dc,Ts,'statename',states,'inputname',inputs,'outputname',output
s);

t = 0:0.005:7;
rc =0.2*ones(size(t));
[y,t,x]=lsim(sys_cl,rc,t);
[AX,H1,H2] = plotyy(t,y(:,1),t,y(:,2),'plot');
set(get(AX(1),'Ylabel'),'String','cart position (m)')
set(get(AX(2),'Ylabel'),'String','pendulum angle (radians)')
title('Voltage Step Response Digital LQR Control')
```

Appendix Ic – Force to Current graph

```
x=[2.075,2.9,5.375,7.15,8.475,10.95,12.9,15.75,17.45,20.5]
y=3:12
p=polyfit(x,y,1)
xfit=2:20.5
yfit=p(1)*xfit+p(2)
plot(xfit,yfit,x,y,'o')
xlabel('Force [N]');
ylabel('Current [A]');
legend('fitted curve','recorded data','Location','NorthWest')
text(10,6.5,'y = 0.482x + 2.51')
```

Appendix Id – Open Loop Step response

```
%% System Parameters
clear all
clc
m = 0.277;          %kg
l = 0.434;          % m %centre of gravity length
M = 1.3032;         % kg
Ip= (1/3)*m*(l^2);  % kg*m^2
g = 9.80655;        %m/s^2 or N/kg
b = 5;              %N*s/m
Ts=0.005;
s=tf('s');

p=(m*l)^2-(M+m)*(Ip+m*l^2);

% CART OLTF
TF_c=((m*l*g/p-((Ip+m*l^2)/p)*s^2))/(s^4-
(b*(Ip+m*l^2)*s^3)/p+((M+m)*m*g*l*s^2)/p+(m*g*l*b*s)/p)
%cart plant in continuous
pc=pole(TF_c);
TF_cd = c2d(TF_c,Ts,'zoh');

% PENDULUM OLTF
TF_p  =  (m*l*s/p)/(s^3-(b*(Ip+m*l^2)*s^2)/p+((M+m)*m*g*l*s)/p+(m*g*l*b)/p)
%pend plant in continuous
po=pole(TF_p);
TF_pd = c2d(TF_p,Ts,'zoh');
```

```
TF_pc=(m*g*l-(Ip+m*l^2)*s^2)/(m*l*s^2)
TF_pcd = c2d(TF_pc,Ts,'zoh');

%% TF
sys_tf = [TF_c; TF_p]

inputs = {'F'};
outputs = {'x';'phi'};

set(sys_tf,'InputName',inputs);
set(sys_tf,'OutputName',outputs);

sys_tf %from inpput F to output x/phi

%% OL IMPULSE RESPONSE
sys_tf = [TF_c; TF_p]

inputs = {'F'};
outputs = {'x';'phi'};

set(sys_tf,'InputName',inputs);
set(sys_tf,'OutputName',outputs);

t = 0:0.005:5;
impulse(sys_tf,t);
title('Open Loop Impulse Response');
%the system response is unstable in open loop

%% OL Step response
t = 0:0.005:10;
u = ones(size(t));
[y,t] = lsim(sys_tf,u,t);
plot(t,y);
axis([0 3 -100 100]);
title('Open Loop Step Response');
legend('x','phi');

step_info=lsiminfo(y,t);
cart_info=step_info(1)
pend_info=step_info(2)
```

Appendix Ie - Force to Current Dead Zone Account

```
function I = fcn(F)
if F>1 %0.8
    I=0.482*F+2.51
else if F<-1 %0.5
        I=0.482*F-2.51
    else
        I=0
    end
end
```

Appendix II – Project Organization

Data Acquisition

To acquire the needed data for finding the Transfer Function, the discrete time sampling, the suitable controller and the general unknown parameters that are needed for the achievement of the goal, extensive literature research and experimental setups were implemented.

The unknowns in terms of the Transfer function of the system are the cart friction coefficient, the pendulum friction coefficient and the moment of inertia of the pendulum and the cart.

Based on the findings of other similar research papers, the friction between the pendulum and the cart system is negligible because of its lubrication. However, in [22] the pendulum friction is approximated. A similar method, most probably, will be used in order to find the same unknown for this setting.

Type of Modelling

The types of modelling in this paper are the Euler-Lagrange, Mechanical, Mathematical as well as the State Space Modelling. Based on the mechanical modelling of the pendulum, a state space representation will be deduced which will characterize the system by using the existent states.

Risk analysis / feasibility

It is important to mention the fact that the system has a lot of unknowns which need a certain algorithm to be answered. Literature research is the tool needed to be able to do that and to decide on which controller behaves the best. It is expected that several controller designs (linear as well as non-linear ones) will be tested with the goal of stabilizing the system in the fastest way.

Cycle Choice/Design Steps

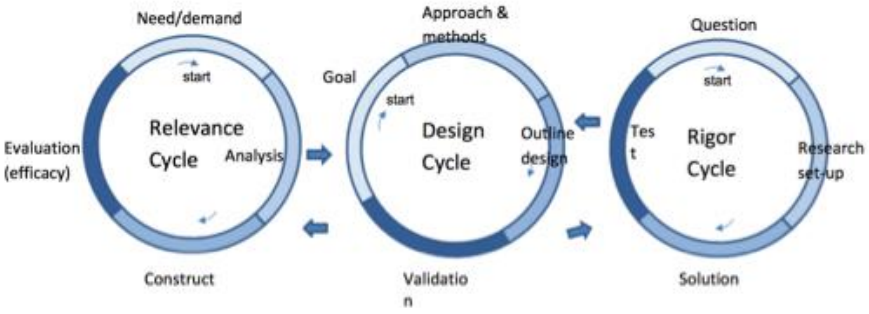

Figure 22: Hevner – Three Cycles - 2007 [21]

The design steps needed to solve and answer the main research question are related to the Cycles of Hevner taught during the Research & Design Methodology course:

After analysing the cycles and their application, a decision of using each for a specific research part has been taken.

The Relevance Cycle is applicable to this research as the acceptance criteria of the desired design output will be specified. The IP has to be stabilized and this stabilization will indeed improve the environment by bringing in a more thorough and specialized research of the chosen controller applied to this system [21]. These acceptance criteria have to do with the research question formulation and answering.

Based on the research questions, a need for finding the best controller is present. Experimental setups are required to find the friction factor and efficiency of the motor. Hereby, the Rigor Cycle is used for this part. A controller will be chosen after answering all the research questions and by also using information from previously written research papers as well as experimenting to see how the actual controller behaves with the real-time plant.

The last and the most important cycle is the Design one which is the heart of the research project and is the Cycle applied throughout the thesis. The requirements and hereby the research questions are the inputs from the relevance cycle, and the experiments, design, evaluation theories and methods are drawn from the rigor cycle. The chosen controller therefore the artefact of the system and its performance will be evaluated by the end of the thesis.

Planning 2nd Block

In order to be able to finish the project successfully, an amount of 9-10 hours per day to solve the stabilization problem were needed. As from the 1st of April, the actual research began, and each research question was solved and the build-up knowledge was acquired which helped with reaching the final goal.

Week vs Task	Parameter Identification (Experiments, Simulations, Literature Research)	Controller Selection & Design	Testing	Corrections & Adjustments
Week 14				
Week 15				
Week 16				
Week 17				
Week 18				
Week 19				
Week 20				
Week 21				
Week 22				
Week 23				
Week 24				
Week 25				

Table 8: Weekly Schedule

Appendix III – Parameter Definition

Appendix IIIa - Encoder

It is attached directly to the motor shaft and translates the rotary motion of the shaft into a two-channel digital outputs which are two square waves in quadrature A & B. These index outputs are 90 degrees out of phase. A high true index pulse is generated once for each full rotation of the code-wheel. The most often used term for resolution is the Pulses per Revolution (PPR) which is equal to Cycles per Revolution [5].

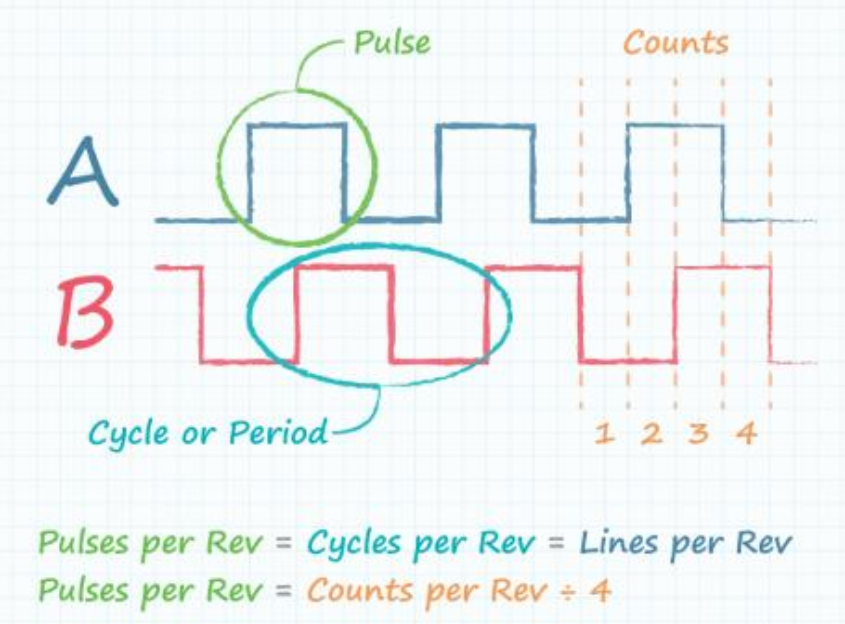

Figure 23: Comparison between typical datasheet waveform drawings and figures [5]

The principle of the used encoder is as follows: the output of the encoder is connected to the dSPACE hardware converter which sends the information to the controller. A pulse is generated once for each full rotation of the shaft. A LED diode (light source) creates a light beam that passes through a disc plate that is attached in the DC motor shaft (Figure 24).

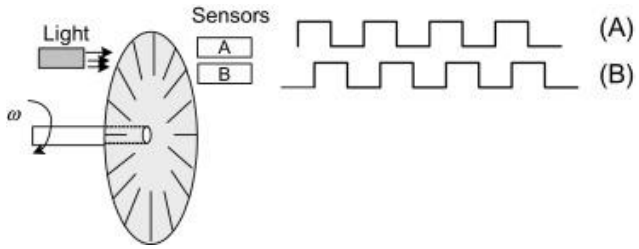

Figure 24: The structure of an optical encoder showing sensor A and B outputs [9]

As the readout of the encoder is in $Cycles\ per\ Revolution = PPR$, both the Encoder Position and Speed are being read through the dSPACE Hardware System and then multiplied by the gains, (A) and (B) respectively. The final position as well as speed can be observed in the Simulink file as seen in Figure 3. The encoder readout is digital which means that no A/D conversion is needed, and the readout values go directly to the controller after being multiplied with the gain.

The PPR's relation to Counts per revolution (CPR) can be obtained as follows based on Figure 23:

$$CPR = PPR \times 4 = 500PPR \times 4 = 2000CPR \quad (0)$$

Therefore, both $500\ PPR$ and $2000\ CPR$ are the resolutions of this encoder just given in different types of systems.

The amount of mechanical degrees or radians for each pulse is equal to:

$$Degree\ of\ Resolution = \frac{360^\circ}{500\ pulses} = 0.72\ mechanical\ degree\ for\ each\ pulse \quad (A)$$

$$Radians\ of Resolution = \frac{2\pi}{500\ pulses} = 0.01257\ radians\ for\ each\ pulse \quad (B)$$

In order to find the required gain to translate the encoder readout from cycles (pulses) to meters, equation the meter per pulse relation is needed which is given by:

$$MPP = Position\ Gain = \frac{2\pi r_m}{500\ pulses} = 0.000327 \frac{m}{pulse} \quad (C)$$

Where $r_m = 0.026\ m$ is the radius of the rotating shaft that is connected to the rail.

Furthermore, as the encoder offers information about the angular velocity in cycles per revolution (PPR), a relation between the angular velocity and the translational velocity can be deduced based on the sampling time chosen for the converter which in this case is $T_s = 0.005\ sec$.

$$Velocity\ Gain = \frac{MPP}{T_s} = 0.0654 \frac{m}{s \times pulse} \quad (D)$$

The Pulses per Meter (PPM) can be used to find the amount of pulses per length of rail [31]:

$$PPM = \frac{PPR}{2\pi \times r} \quad (E)$$

$$Pulses\ per\ length = PPM \times L_{Effective} \quad (F)$$

The resolution per meter represents the resolution in cart position and is sometimes needed to see how many counts or pulses are included in a certain length. It can be found by making use of the following relation:

$$PPM_{theoretical} = \frac{500\ pulses}{2\pi r_m} = 3060.73 \frac{pulses}{m} \qquad (G)$$

$$Resolution = \left(L_{RailEffective} - L_{Cart}\right) \times PPM = L_{Effective} \times PPM$$
$$= 0.87m \times 3060.73 \frac{pulses}{m} = 2662.84\ pulses \qquad (H)$$

Where $L_{Rail\ Effective}$ is the length that the cart can travel excluding the cart length itself until the switch from $[-0.5; 0.5]\ m$ is turned on.

This value for the theoretical PPM can be validated from the outcome of an experiment where the output of the encoder is registered for the whole length of the rail. Based on the obtained counts, and the effective length of the rail minus the cart length, a resolution for the whole Effective Rail Length can be obtained.

The total amount of pulses that the readback of the encoder gave for the whole length of the rail is $4730.5\ pulses$. It should be mentioned that the cart length influenced the readout, and it which should be subtracted from the actual length of the rail. Therefore, by knowing the actual length of the rail and that of the cart $L_{Rail} = 1.67\ m, L_{Cart} = 0.13\ m$, the experimental PPM value is:

$$PPM_{experimental} = \frac{4730.5\ pulses}{1.54\ m} = 3071.75 \frac{pulses}{m} \qquad (I)$$

This value is very close to theoretical one which shows that the encoder works as expected.

Appendix IIIb - Potentiometer

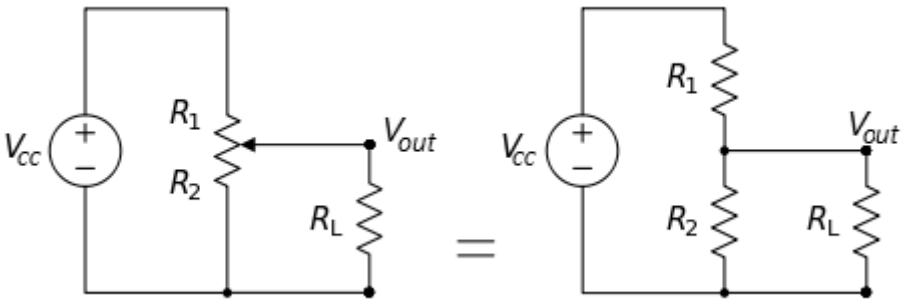

Figure 25: Potentiometer Electrical Circuit [23]

The most common types of pots are three-terminal resistors with an electrical contact that either slides or rotates along a resistor (or in some cases between different

resistors) in a voltage divider circuit to provide variable resistance (and variable voltage output) [33]. Figure 25 shows in detail the Electrical Circuit of the three-terminal potentiometer that behaves as a Voltage divider, where the Voltage source is $\pm 10\ V$ in the current setting.

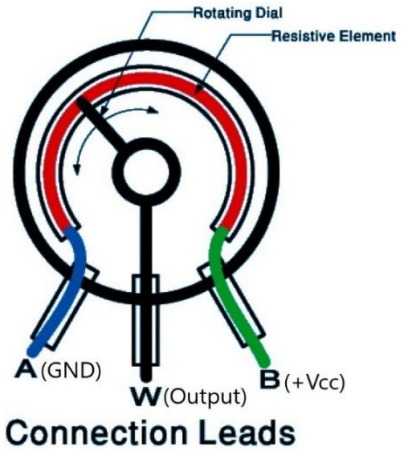

Figure 26: Potentiometer Connection Diagram [33]

The main advantages of potentiometers are the prices being economical, the device is easily implemented, and the body length is relatively short. As seen in Figure 26, a mechanical contact between the Resistive Element and the Rotating dial is needed to provide position feedback. Thus, potentiometers are known to have poor repeatability, larger hysteresis and can be affected by noise (non-ideal effects). Due to the contact wear, the output W (Figure 26) tends to deteriorate over time, particularly in high vibration conditions [44].

An important aspect is that the physical system needs to be well calibrated. Thus, the calibration of the potentiometer was made by adding a value of -0.023 to the Angle Voltage output which would make the Voltage at the upright position of the pendulum to be equal to $0\ V$.

The used equation to determine the output voltage which is smaller than the input one is given by:

$$V_{out} = V_{cc} R_L \qquad (J)$$

Where

$$R_L = \frac{R_2}{R_1 + R_2} \qquad (K)$$

Resolution is characterized as the minimal amount by which the voltage changes in response to a corresponding shaft movement. Several additional advantages of potentiometers are that the resolution is virtually infinite, and it is an absolute position sensing device. Furthermore, the potentiometer always knows where it is positioned (independent of being powered on or off) and does not need to return to zero, as it usually is in the case of using other incremental position sensing devices [25].

The range of values that the potentiometer has as outputs are from $[-10;\ +10]\ V$ with some deviations as for example the Resting downward position of the Pendulum has the value of $-10.23\ V$ while the straight upward position has the value of $-0.23\ V$, which is accounted for by the Simulink Calibration constant as shown in Figure 27.

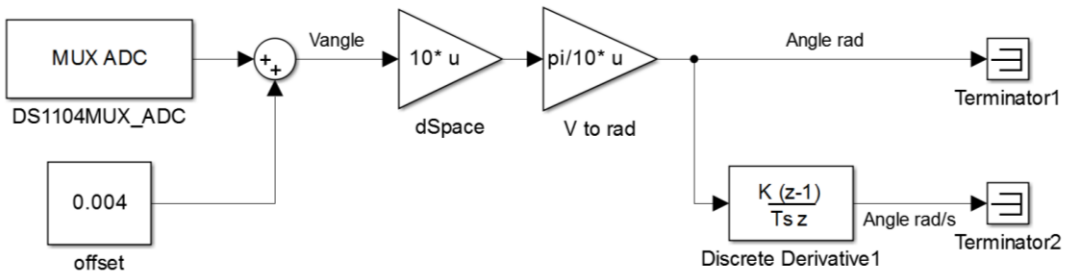

Figure 27: Simulink Potentiometer Angle Acquisition and Calibration

Based on the total range of Volts which is $20\ V$ the constant which shows the Resolution expressed in Radians per Volt can be found:

$$Resolution = \frac{2\pi}{Range} = \frac{2\pi}{20V} = 0.314\frac{rad}{V} \qquad (L)$$

Therefore, $10\ V$ translates to $2\pi\ radians\ = 180\ degrees$.

In order to get the most accurate and sampled reading from the potentiometer the W terminal is connected to the $16 - bit$ input of the A/D Converter. As the dSPACE A/DC is a Multiplex type of converted the pendulum angle was chosen as the most important parameter to be acquire by use of the 16-bit connection.

Appendix IIIc – Shaft to Rail Translation

To find the radius of the bearing, the starting point of the outer shaft coming from the motor (Figure 28) together with the toothed rail was analysed. For one turn of the motor shaft the distance travelled by the rail was recorded. Therefore, based on the formula of the length of a circle $L_{circle} = 2\pi \times r_m$, the recorded length travelled by the rail in one turn is $16\ cm = 0.16\ m$, which resulted in a $r_m = 0.0255\ m \sim 0.026\ m$.

Figure 28: Motor Shaft output

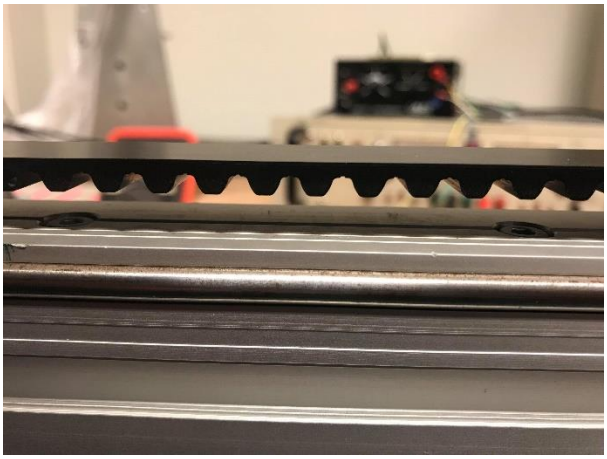

Figure 29: Toothed Rail

Figure 30: Motor to pulley and toothed belt coupling

Appendix IIId – Cart Mass

Due to the fact that the cart could not be disassembled in order to be weighted, an approximation about its mass was made.

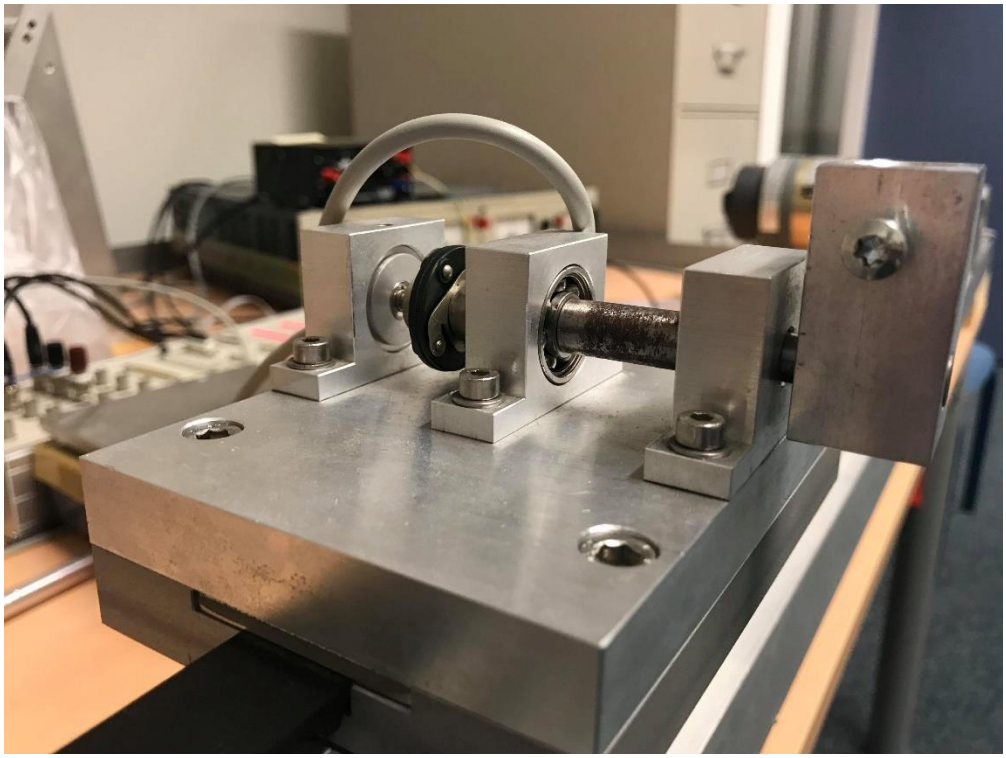

Figure 31: Upper part of the cart

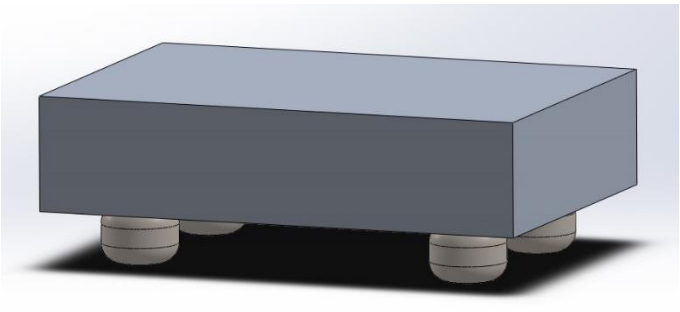

Figure 32: Assembled Cart

The cart is made of three components:

- ➔ Upper part which attaches the pivot point of the pendulum and the potentiometer (could be detached and weights 213.7 g)
- ➔ Main cart body made of Aluminium ($\rho = 2.7 \frac{g}{cm^3}$)

➔ 4 Stainless Steel wheels with the help of which the cart slides on the rail ($\rho = 7.8\frac{g}{cm^3}, filling\ factor = 0.7$)

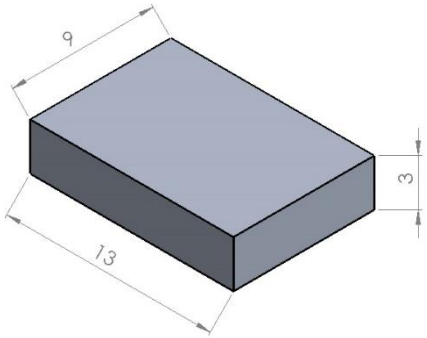

Figure 33a: Cart Dimensions

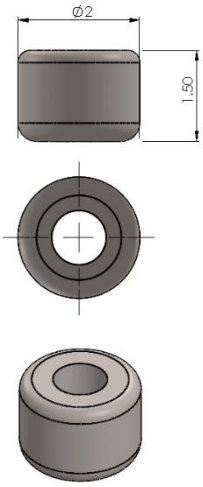

Figure 33b: Wheel Dimensions

The real-life dimensions of the cart and wheels can be seen in Figure 33a and 33b respectively. The equation of the mass is given as:

$$M = V\rho = wlh\rho = 2\pi rh\rho \qquad \text{(M)}$$

Based on equation M and the additional attachments, the mass of the cart is calculated to be equal to 1303.2 g.

Appendix IV

The DC-motor's characteristics are provided by the producer. The dSPACE software and real-time interface provides a limited maximum value of the samples per time unit that can be used for the real-time control timing. The physical values of mass and length are measured with a ruler as well as weighting mechanism. The value for friction (viscous, static, Coulomb), which is going to be incorporated into the b friction coefficient from the Euler-Lagrange equations, will be identified from an experimental setting that is going to be discussed further on in the report. For the experiment a dynamometer, the cart system together with the toothed rail will be used.

Appendix IVa - Frequency domain (Laplace)

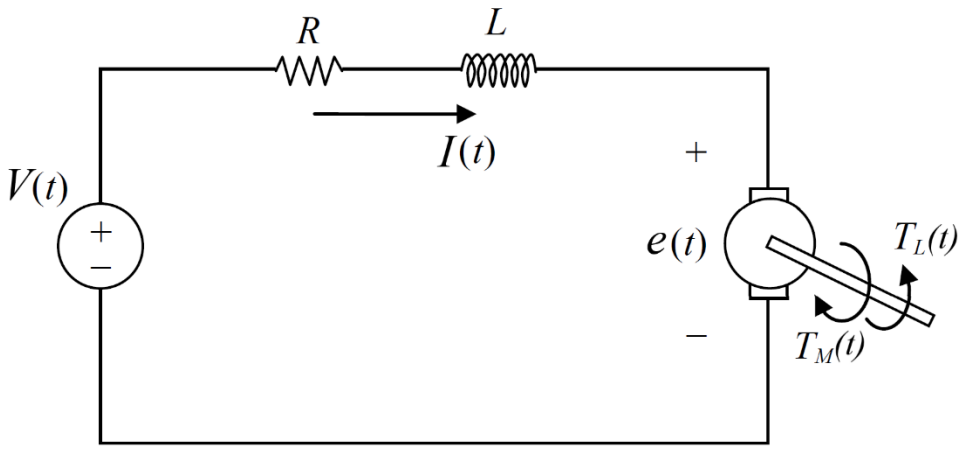

Figure 34: Electrical Circuit of the DC Motor

As seen in Figure 34, Kirchhoff's Voltage Law (KVL) of the Electrical Circuit is given by:

$$v(t) = RI + L\frac{dI}{dt} + e \qquad (N)$$

where $v(t)$ is the input voltage, R & I are the Resistance and the Current of the Armature, L the inductance of the armature's windings, and v_b is the back electromotive force (E.M.F.).

Its Laplace form is given by:

$$V(s) = RI(s) + sLI(s) + E(s) \qquad (O)$$

From Faraday's Law:

$$\tau_m = k_T k_g I \qquad (P)$$

$$e = k_e \omega_m = k_e \frac{d\theta_m}{dt} \qquad (Q)$$

As $k_g = 1$ the Laplace of both equations is:

$$T_m = k_T I(s) \qquad (R)$$

$$E(s) = k_e W_m(s) = s k_e \theta_m(s) \qquad (S)$$

Furthermore, the Mechanical Components (Figure 5) are expressed by:

$$\tau_m = \tau_L + B\omega_m + J\frac{d\omega_m}{dt} \qquad (T)$$

Where τ_L is the external load torque and it is present only when the motor is used to drive and external load. It is expressed as:

$$\tau_L = r_m F \qquad (U)$$

In the modelling of the relationship between the motor and the input voltage coming from the power amplifier, the external load is ignored.

The Laplace is therefore given by:

$$T_m(s) = sb\theta_{\mathrm{m}}(s) + s^2 \mathrm{J}\theta_{\mathrm{m}}(s) \qquad (V)$$

By combining (O) to (V) together the Transfer Function relating the input voltage $V(s)$ and the output speed $W(s)$ is obtained as follows:

$$W_m(s) = \frac{k_T}{(sJ + B)(sL + R) + k_T^2} V(s) \qquad (W)$$

The equation can be further simplified since $L \ll J$, as well as due to the fact that the current does not vary in time and is constant $\frac{dI}{dt} = 0$. Thus, it results that:

$$\frac{W_m(s)}{V(s)} = \frac{G_1}{Ts + 1} \qquad (X)$$

where G_1 is the gain of the DC Motor and T is the time constant given by the equations:

$$G_1 = \frac{k_T}{BR + k_T^2} \qquad (Y)$$

$$T = \frac{JR}{BR + k_T^2} \qquad (Z)$$

Equation (T) and (U) makes it possible to relate the input voltage to the force acting on the cart.

The parameters that are known can be found in table 9:

Symbol	Value
R	$1.1\ \Omega$
I	$6.7\ A$
L	$< 10^{-4}\ H$
v_b	$18.6\ V$
k_T	$0.0592\ N \times m/A$
k_e	$0.0592\ V \times \frac{s}{rad}$
J	$3.5 \times 10^{-5}\ kg \times m^2$
B	$2.3 \times 10^{-4} N \times m \times \frac{s}{rad}$
r_m	$0.026\ m$
T	$10.2 \times 10^{-3}\ s$

Table 9: Known Parameters

Equation (X) has been obtained as the one connecting the angular velocity of the motor shaft that drives the cart to the voltage input to the motor in terms of the Laplace transform. Since the time constant is given by the motor specifications, a check of the value has been carried out by using (Z) and the values from Table to make sure that the parameters are well used and indeed a value of $T = 0.0102\ s$ has been obtained, which is the same as the provided one (Table 1). The value for G_1 was calculated as $G_1 = 15.755$. Thus, the relation between angular velocity and voltage is:

$$\frac{W_m(s)}{V(s)} = \frac{15.755}{0.0102s + 1} \tag{A1}$$

Appendix IVb - Time domain

By using the Electrical Circuit given by Kirchhoff's Voltage Law (KVL) from equation (O), Faraday's Law given by equation (P) and the Mechanical Component equation given by (T) and (U) the overall connection between all the needed elements is obtained. As before, the small effect of the motor Inductance is ignored [34] and the angular velocity of the cart is given by:

$$\omega_m = \frac{k_g}{r_m}\dot{x} \tag{A2}$$

Which results in:

$$\tau_L = k_T k_g I - B\frac{k_g}{r_m}\dot{x} + J\frac{k_g}{r_m}\ddot{x} \tag{A3}$$

Rearranging the equation gives:

$$F = \frac{k_T k_g}{r_m} I - \frac{B k_g}{r_m^2}\dot{x} - \frac{J k_g}{r_m^2}\ddot{x} \tag{A4}$$

From (O), (P) and (Q) it results that:

$$V = RI + \frac{k_e k_g}{r_m}\dot{x} \tag{A5}$$

Thus, the Force and Voltage can be combined from eq. (A4) and eq. (A5) by:

$$F = \frac{k_T k_g}{r_m R} V - \left(\frac{k_T k_g^2 k_e}{r_m^2 R} + \frac{B k_g}{r_m^2}\right)\dot{x} - \frac{J k_g}{r_m^2}\ddot{x} \tag{A6}$$

[53] validates the relationship obtained in eq. (A6).

Appendix V

Appendix Va - LQR

The finite horizon, linear quadratic regulator (LQR) problem is a very commonly used technique for solving optimal control problems. In the case of this thesis, it has been chosen as the most promising technique to stabilize the system and to achieve the upward position of the pendulum. The Dynamical model and its dimensions is given as follows:

$$\dot{x} = Ax + Bu,\ x \in R^{n\times 1}, u \in R^{p\times 1}, A \in R^{n\times n}, B \in R^{n\times p}$$

$$y = Cx, C \in R^{m\times n}$$

The LQR Method aims at finding the optimal control law which minimizes the J quadratic cost function:

$$J = \int_0^\infty \left(x^T(t)Qx(t) + u^T(t)Q_R u(t)\right)dt \tag{A7}$$

With $Q \geq 0$, $Q_R > 0$ being symmetric, positive (semi-) definite matrices where

$Q \in R^{n\times n}$ and $Q_R \in R^{1\times 1}$ it is guaranteed that a solution exists. The input, and therefore the solution to the LQR problem is given by the linear control law u of the form

$$u = -Kx = -{Q_R}^{-1}B^T Px \tag{A8}$$

Where $K = {Q_R}^{-1}B^T P$, $K \in R^{1\times n}$ is the optimal feedback gain matrix, $P > 0$, $P \in R^{1\times 1}$ is a positive definite constant matrix that satisfies the Algebraic Riccati equation and is its solution:

$$PA + A^T P + Q - PBR^{-1}B^T P = 0 \tag{A9}$$

If the system is reachable, it can be shown that there is a unique positive definite matrix P satisfying equation (A9) that makes the closed loop system stable. This quadratic equation can be solved numerically: in MATLAB the command $K = lqr(A, B, Q, Q_r)$ provides the optimal feedback compensator. One of the most important questions in LQR design is how to choose the weights Q and Q_R. For the choice of the diagonal weights, each individual diagonal element describes how much each state and input should contribute to the overall cost. Thus, high weights to states that should remain small can be given [27].

$$Q = \begin{bmatrix} q_1 & 0 & 0 \\ 0 & \ddots & 0 \\ 0 & 0 & q_2 \end{bmatrix} \tag{A10}$$

Commonly, a trial and error method has been used to select the elements of Q and Q_R matrices. When adjusting the weights of the Q matrix, also called State Cost, different types of behaviours of the system can be analysed.

As mentioned before in section 2.4.1.4, the control is carried out by a discrete time controller which means that the (LQR) should be implemented in a sampled setting. This implementation will be shown in the following section.

After identifying the coefficients of the K matrix, the closed-loop matrixes (as seen in figure 35) are given by:

$A_c = A - BK$

$B_c = B$

$C_c = C - DK$

$D_c = D$

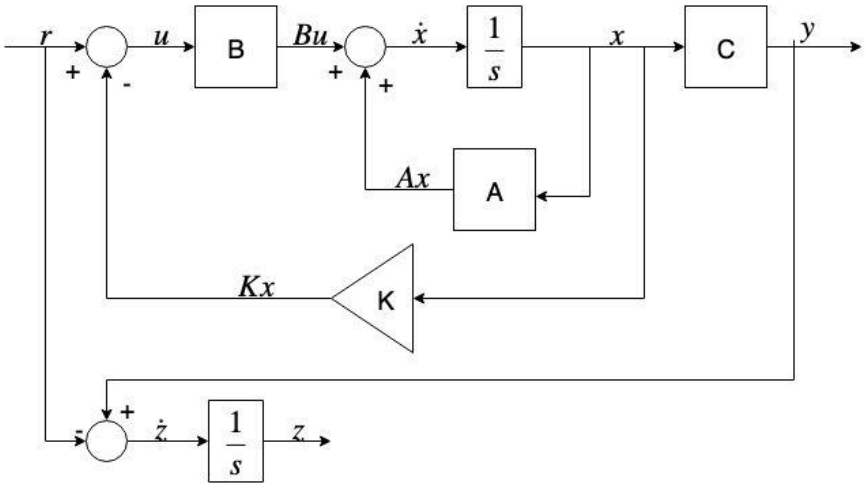

Figure 35a: Continuous State Space Closed-Loop Feedback LQR Representation

After discretization, the Closed loop matrixes become:

$A_c = A_d - B_d K$

$B_c = B_d$

$C_c = C_d - D_d K$

$D_c = D_d$

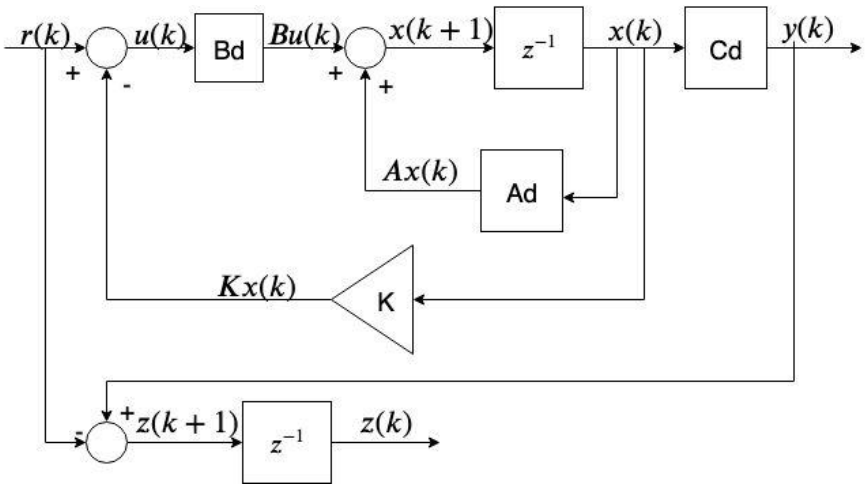

Figure 35b: Discrete State Space Closed-Loop Feedback LQR Representation

Appendix Vb

Transfer Function

The frequency domain representation is needed to analyse the open-loop behaviour of the system and can also be used for the tuning of the Proportional Integral Derivative (PID) controller if a PID controller is implemented.

Taking the Laplace Transforms of eq. (11) & (12):

$$(M+m)s^2X(s) + mls^2\theta(s) = F_{cart}(s) - bsX(s) \qquad (A11)$$

$$mls^2X(s) + \left(I_p + ml^2\right)s^2\theta(s) - mgl\theta(s) = 0 \qquad (A12)$$

By rearranging eq. (A11):

$$X(s) = \frac{F_{cart}(s) - mls^2\theta(s)}{(M+m)s^2 + bs} \qquad (A13)$$

And by rearranging eq. (A12):

$$\theta(s) = \frac{mls^2}{mgl - \left(I_p + ml^2\right)s^2}X(s) \qquad (A14)$$

To get the relation between the pendulum angle and the Force $X(s)$ from eq. (A14) is replaced with the one from eq. (A13) and the transfer function becomes:

$$\frac{\theta(s)}{F_{cart}(s)} = \frac{mls}{[(ml)^2 - (M+m)\left(I_p + ml^2\right)]s^3 - b\left(I_p + ml^2\right)s^2 + mgl(M+m)s + bmgl} \qquad (A15)$$

By taking $y = [(ml)^2 - (M+m)\left(I_p + ml^2\right)]$, eq. (A15) becomes:

$$\frac{\theta(s)}{F_{cart}(s)} = \frac{\frac{ml}{y}s}{s^3 - \frac{b\left(I_p + ml^2\right)}{y}s^2 + \frac{mgl(M+m)}{y}s + \frac{bmgl}{y}} \qquad (A16)$$

For the transfer function between he Cart Position and the Input Force similarly $\theta(s)$ is replaced from eq. (A13) with the one from eq. (A13):

$$\frac{X(s)}{F_{cart}(s)} = \frac{mlg - \left(I_p + ml^2\right)s^2}{[(ml)^2 - (M+m)\left(I_p + ml^2\right)]s^4 - b\left(I_p + ml^2\right)s^3 + mgl(M+m)s^2 + bmgls} \qquad (A17)$$

$$\frac{X(s)}{F_{cart}(s)} = \frac{\frac{mlg - (I_p + ml^2)}{y}s^2}{s^4 - \frac{b(I_p + ml^2)}{y}s^3 + \frac{mgl(M+m)}{y}s^2 + \frac{bmgl}{y}s} \quad (A18)$$

And based on both transfer function the relationship between $X(s)$ & $\theta(s)$ is given by:

$$\frac{X(s)}{\theta(s)} = \frac{mgl - (I_p + ml^2)s^2}{mls^2} \quad (A19)$$

After using the known parameters, the values for each transfer function are given by:

$$\frac{\theta(s)}{F_{cart}(s)} = \frac{-1.2591s}{s^3 + 3.6431s^2 - 19.5121s - 61.7392} \quad (A20)$$

Appendix VI

Ramp Experiment

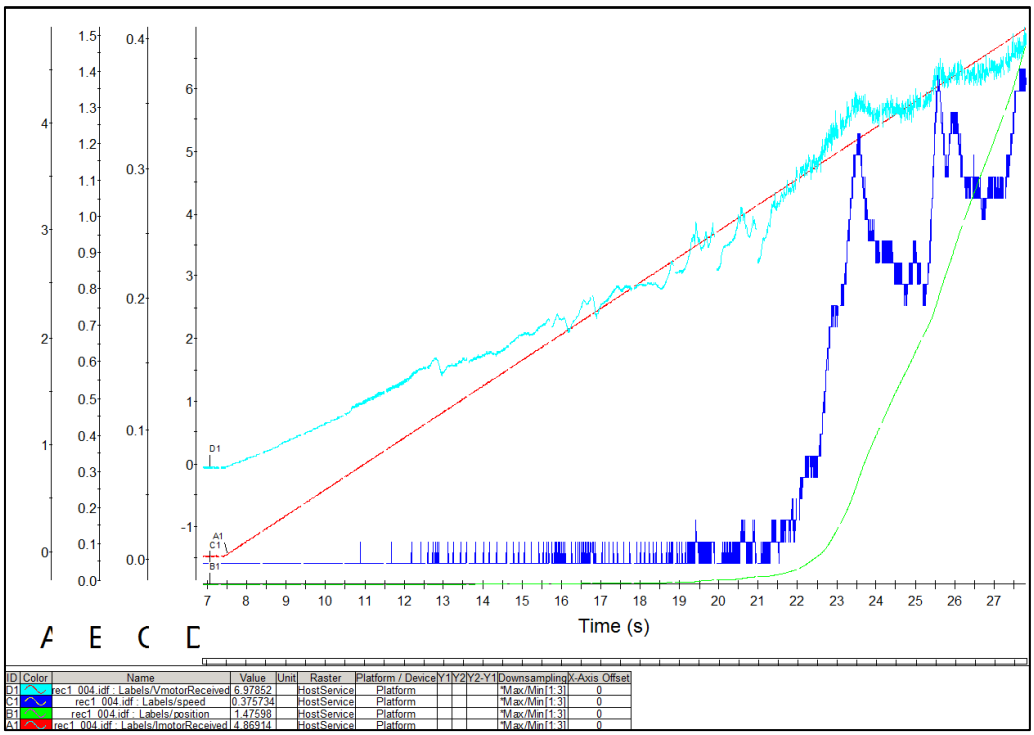

Figure 36: Current Ramp Experiment

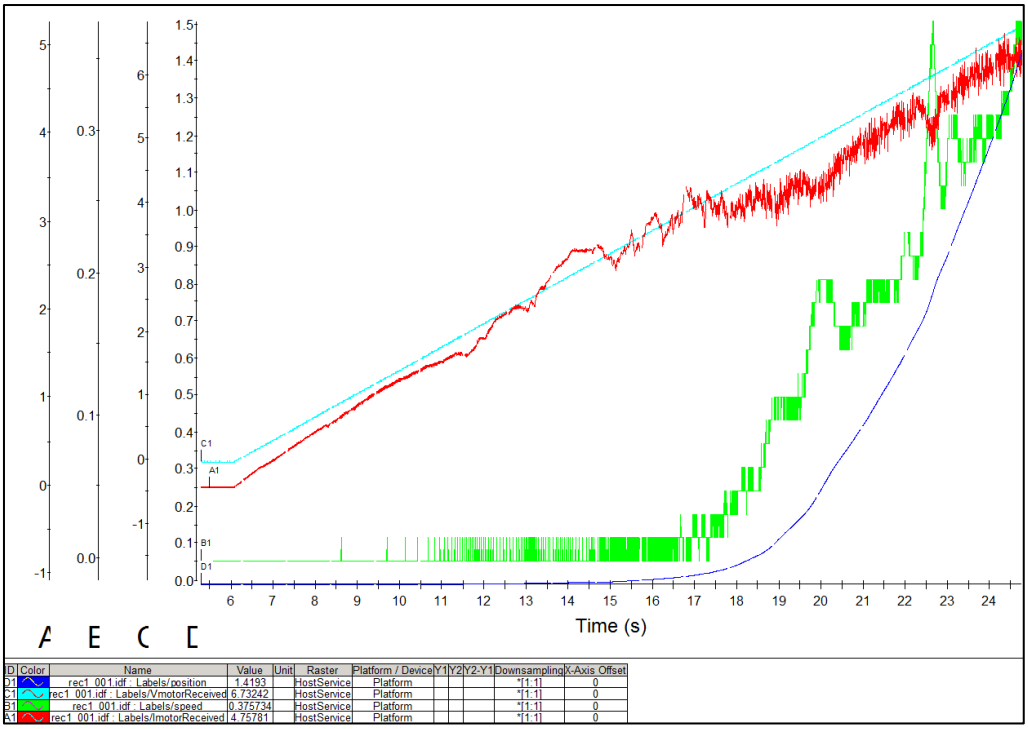

Figure 37: Voltage Ramp Experiment

After carrying out both experiments, the presence of the non-linearity and the effect of frictional forces within the system can be visualised.